DOI:
10.1109/TFUZZ.2024.3370995

Document Version
Peer reviewed version

Observer-based fuzzy tracking control for an unmanned aerial vehicle with communication constraints

Linghuan Kong, Zhijie Liu, *Member, IEEE*, Zhijia Zhao, *Member, IEEE*, and Hak-Keung Lam, *Fellow, IEEE*

***Abstract*—We investigate the trajectory tracking problem of underactuated aerial vehicles with unknown mass in the presence of unknown non-vanishing disturbances using an event-triggered approach, while considering the constraint that the derivative of the reference trajectory is not available. In contrast to existing references where the derivative of the reference trajectory is needed, here we first introduce a high-gain observer to estimate the unknown derivative solely from the reference trajectory. A disturbance observer is designed to compensate for non-vanishing disturbances, such as wind, etc. Fuzzy logic systems are used to approximate the model uncertainty arising from the unknown mass of the vehicle, and then we derive a thrust command law that follows from a desired stabilizing force. Additionally, unlike traditional fixed and relative threshold strategies that rely solely on control signals, we develop a new time-varying event-triggered mechanism linked to the performance of the controlled system, taking into account factors such as tracking errors, to develop angular velocity commands, enhancing tracking accuracy while efficiently conserving communication resources, especially in the absence of Zeno behavior. We present simulation results to demonstrate the efficacy of the proposed approach and validate the theoretical findings.**

***Index Terms*—Disturbance observers; fuzzy logic systems; event-triggered control; model uncertainty; underactuated autonomous aerial vehicles.**

I. Introduction

Over the past few decades, there has been remarkable progress in the development of aerial robots, particularly small unmanned aerial vehicles (UAVs) and drones [1], [2]. These advancements have encompassed various aspects, including their design, operational techniques, flight capabilities, and navigation control. UAVs are now extensively applied in a diverse array of services, including but not limited to aerial photography, route optimization, search and rescue missions, as well as the inspection of power lines and civil infrastructure projects [3], [4]. The quadrotor UAVs consist of four independent controlled rotors which enable them to perform landing and take-off vertically [5]. However, due to the characteristics of nonlinearities, strong couplings, and underactuation, etc., it is significantly difficult to design a highly accurate controller. In addition, unexpected disturbances, including wind and blade flapping, etc., as well as model uncertainty render the controller design more challenging. The paper aims to provide a feasible solution using an event-triggered approach to the trajectory tracking problem of a quadrotor UAV with unknown mass in the presence of non-vanishing disturbances.

Many interesting and significant references have been reported to contribute to the development of UAVs. For instance, [6] presented a robust nonlinear control system tailored for UAVs with unknown constant disturbances. In [7], a method for position regulation in UAVs was put forth, operating under the assumption of a known mass and considering that aerodynamic disturbances dissipate in relation to the system's translational kinetic energy. In [8], [9], global tracking control of thrust-vectoring UAVs were developed, respectively, which requires the controlled system to be disturbances free, and where the mass of the vehicle is known. In [10], a robust tracking controller, grounded in a learning-based approach, was formulated for aerial robots operating in the presence of vanishing disturbances. In [11], [12], a nonlinear model predictive control algorithm is applied to the tracking control of UAVs, where the external disturbance is presented. However, the mass of UAVs is assumed known. UAVs frequently operate in challenging and intricate conditions, encountering time-varying, aperiodic, and persistent disturbances such as wind, etc., which hinder the improvement of the tracking performance. The studies cited, including [6]–[12], demonstrated viable outcomes in the tracking control for UAVs. However, their applicability is constrained as they presume knowledge of UAV mass and assume external disturbances to be either constant or gradually vanishing. This limitation clearly narrows down their suitability for addressing challenges in intricate operational environments.

In general, it is of vital importance for the realization of tracking control to derive complete knowledge of the reference trajectory and its derivative [13]–[15]. In the practical scenario of UAVs tracking a mobile target, the real-time acquisition of the target's position is facilitated by a measurement device. Importantly, this information is not known to UAVs in advance,

This work was supported in part by the National Natural Science Foundation of China under Grant 62073030, and Grant 62273112, in part by the the Joint Fund of Ministry of Education for Equipment Pre-Research under Grant 8091B03032303, and in part by the Science and Technology Planning Project of Guangzhou under Grant 202201020185 and Grant 2023A03J0120. The work of Linghuan Kong was supported by the UM Postdoctoral Fellow Scheme under the UM Talent Programme. (*Corresponding author:* Zhijie Liu)

Linghuan Kong is with the Department of Electrical and Computer Engineering, Faculty of Science and Technology, University of Macau, Macau, China. (e-mail: kong.ahuan@gmail.com)

Zhijie Liu is with the School of Intelligence Science and Technology, University of Science and Technology Beijing, Beijing 100083, China. (e-mail: liuzhijie2012@gmail.com)

Zhijia Zhao is with the School of Mechanical and Electrical Engineering, Guangzhou University, Guangzhou 510006, China. (e-mail: zhjzhaoscut@163.com)

Hak-Keung Lam is with the Department of Engineering, King's College London, Strand, London, WC2R 2LS, United Kingdom. (e-mail: hak-keung.lam@kcl.ac.uk)

meaning UAVs lack prior knowledge before data transmission, which is prevalent in sectors like aerial photography [16], target surveillance [17], and various civil and military applications, exemplifying the dynamic nature of real-world tracking challenges. It is crucial to note that the velocity of the mobile target is also unavailable, implying that the derivative of the reference trajectory remains unknown to UAVs. Obtaining comprehensive knowledge of both the reference trajectory and its derivative is crucial for the successful implementation of tracking control, as emphasized in [13]–[15]. Even though there exist many interesting results to focus on the tracking control of UAVs, such as [18]–[21], for the practical scenario of UAVs tracking a mobile target mentioned earlier, the unavailability of the derivative of the reference trajectory poses a challenge, making it impractical to directly apply the algorithms established in [18]–[21].

Currently, remote real-time control of UAVs is of significant importance for various practical tasks, including aerial photography, route optimization, and search and rescue missions. However, it is constrained by limited communication resources such as energy and network bandwidth, as well as signal delays [22]. To address this challenge, the researchers in [23] proposed three distinct threshold strategies for designing the event-triggered control: the fixed threshold strategy [24], the relative threshold strategy [25], and the switching threshold strategy [26]. However, it is worth noting that the aforementioned three threshold strategies are designed solely based on the control signals, without real-time adjustment according to the performance of the controlled system, such as tracking errors, etc. Generally, while the event-triggered approach saves and mitigates communication resources and burdens, it tends to lose partial information in control signals due to finite samples, resulting in a certain degree of inaccuracy [27], [28]. To enhance the performance, it is highly desirable that the triggering threshold has an explicit relationship with the tracking error, such that the event is triggered frequently when the tracking error is large and less when the tracking error is very small. In this case, the impact of limited communication resources and delays in control signals can be effectively mitigated, while still achieving accurate tracking performance.

Fuzzy logic systems (FLSs) are an effective tool to address model uncertainty of nonlinear systems due to their powerful approximation ability [29]–[32]. In addition, FLSs are also applied to the tracking control of UAVs. For example, in [33], a fuzzy approximator is used to address model uncertainty, and an adaptive fuzzy quantized control scheme is proposed for the tracking control of the quadrotor UAVs. In [34], a fuzzy sliding mode controller is designed for the positioning and path-following of a quadrotor. In [35], an adaptive fuzzy backstepping control method is designed to solve trajectory tracking problems of the quadrotor UAVs. In [36], a fuzzy adaptive nonsingular fixed-time attitude tracking control scheme is proposed for the quadrotor UAVs.

Building upon the aforementioned analysis and discussion, our paper investigates the trajectory tracking control of the quadrotor UAVs with unknown mass in the presence of unknown non-vanishing external disturbances, under the condition that the derivative of the reference trajectory is not available. Compared with [6]–[12], our paper assumes the external disturbance to be unknown and non-vanishing. To address this challenge, we propose a new disturbance observer using FLSs to eliminate the restriction of assuming the disturbance to be vanishing or constant. Moreover, our proposed methods only require nominal information about the quadrotor's mass, eliminating the need for the actual mass. Compared with [18]–[21], we assume, due to practical considerations in tracking mobile targets, that the derivative of the reference trajectory is unknown and not available to the controller. To address this challenge, we introduce a high-gain observer to estimate the derivative of the reference trajectory. This enhancement significantly broadens the applicability of the proposed method, making it suitable for practical tasks in complex environments. Compared to the event-triggered approaches investigated in [23]–[26], we propose a new event-triggered mechanism with a time-varying threshold that depends on the performance of the quadrotor UAVs, including tracking errors. This design ensures that the event is triggered frequently when tracking errors are large, which implies that more control information is applied to the system, leading to better tracking performance. Conversely, when tracking errors are small, it is necessary to decrease the control information applied to the system, and thus longer update intervals are obtained, implying the triggered events are decreased. Therefore, the impact of limited communication resources and delays in control signals can be effectively mitigated, while still achieving accurate tracking performance.

In contrast with existing results, the main contribution of this paper is:

- a new disturbance observer is designed only using FLSs and nominal quadrotor mass, and it can effectively estimate the time-varying and non-vanishing disturbance;
- we introduce a high-gain observer to estimate the derivative of the reference trajectory. This addition enables the application of the proposed algorithm to complex practical tasks, including scenarios such as quadrotor UAVs tracking a mobile target;
- we design a novel time-varying event-triggered mechanism that depends on the performance of the quadrotor. When the tracking error becomes large, the event is triggered frequently, rendering more control information to be applied to the vehicle such that better tracking performance can be obtained. However, when the tracking error is small, the event remains less.

II. Notation

Throughout the paper, $\mathbb{R}^3$ denotes the 3-dimensional Euclidean space. Bold symbols stand for multidimensional variables. The symbol $\mathbf{0}$ denotes a matrix of zeros and $\mathbf{I}$ an identity matrix, both of appropriate dimensions. The transpose operator is denoted by the superscript $(\cdot)^{\mathsf{T}}$. The subscript $(\cdot)_d$ denotes a desired quantity. The set of unit vectors on $\mathbb{R}^3$ is denoted by $\mathsf{S}(2)$. The special orthogonal group of order three is denoted by $\mathsf{SO}(3) := \{\mathbf{X} \in \mathbb{R}^{3\times 3} : \mathbf{X}\mathbf{X}^{\mathsf{T}} = \mathbf{X}^{\mathsf{T}}\mathbf{X} = \mathbf{I},\ \det(\mathbf{X}) = 1\}$. The skew-symmetric matrix associated with a vector $\mathbf{a} \in \mathbb{R}^3$ is denoted by $\mathbf{S}(\mathbf{a})$, such that, given $\mathbf{b} \in \mathbb{R}^3$, the cross product

between $\mathbf{a}$ and $\mathbf{b}$ can be written as $\mathbf{S}(\mathbf{a})\,\mathbf{b}$. Given $\mathbf{x} \in \mathbb{R}^3$, the Euclidean norm is denoted by $\|\mathbf{x}\| := \sqrt{\mathbf{x}^\mathsf{T}\mathbf{x}}$. The operator $\mathrm{diag}(\mathbf{x})$ returns a diagonal matrix with the elements of $\mathbf{x}$ along the main diagonal. Finally, for convenience, $\mathbf{e}_3 := [0,0,1]^\mathsf{T}$ and $\mathbf{1} := [1,1,1]^\mathsf{T}$ are auxiliary vectors. If $\mathbf{A}$ is a real symmetric matrix, $\mathbf{A} \succ 0$ means that $\mathbf{A}$ is positive-definite.

III. Mathematical Preliminaries

A. Coordinate frames and vehicle modeling

To describe the motion of the vehicle, we adopt a fixed inertial frame $\{I\}$ and a body-fixed frame $\{B\}$ attached to the center of mass of the vehicle. The rotation matrix from $\{B\}$ to $\{I\}$ is represented by $\mathbf{R} \in \mathsf{SO}(3)$. The equations governing the kinematics and dynamics of the vehicle are provided by [20]

$$\begin{cases} \dot{\mathbf{p}} = \mathbf{v}, & \text{(1a)} \\ \dot{\mathbf{v}} = \dfrac{1}{m}\mathbf{f} + g\mathbf{e}_3 + \mathbf{d}, & \text{(1b)} \\ \dot{\mathbf{R}} = \mathbf{R}\mathbf{S}(\boldsymbol{\Omega}), & \text{(1c)} \end{cases}$$

where $m \in \mathbb{R}$ is the mass of the vehicle, $g \in \mathbb{R}$ is the net gravitational acceleration, $\mathbf{p}, \mathbf{v} \in \mathbb{R}^3$ represent the position and linear velocity, respectively, both expressed in $\{I\}$, $\boldsymbol{\Omega} \in \mathbb{R}^3$ denotes the angular velocity of $\{B\}$ with respect to $\{I\}$, expressed in $\{B\}$, $\mathbf{f} \in \mathbb{R}^3$ denotes the thrust force vector expressed in $\{I\}$, $\mathbf{d} \in \mathbb{R}^3$ is the external disturbance, such as wind, etc.

The thrust force in a quadrotor vehicle consistently aligns with the vertical axis of the body-fixed frame $\{B\}$, remaining orthogonal to the plane defined by the four rotors. Hence, we can express this as

$$\mathbf{f} = -T\mathbf{R}\mathbf{e}_3, \tag{2}$$

where $T := \|\mathbf{f}\|$ is the net thrust generated by the four motors combined, applied along the direction of $-\mathbf{r}_3 \in \mathsf{S}(2)$, with

$$\mathbf{r}_3 := \mathbf{R}\mathbf{e}_3. \tag{3}$$

To enable the vehicle to execute specific maneuvers, it becomes essential to formulate a desired thrust vector $\mathbf{f}_d \in \mathbb{R}^3$, defined as follows:

$$\mathbf{f}_d := -T_d\mathbf{r}_{3d}, \tag{4}$$

where $T_d := \|\mathbf{f}_d\|$ is the desired net thrust to be applied along the direction of $-\mathbf{r}_{3d} \in \mathsf{S}(2)$. By combining the definitions in (2) and (4), we obtain the following relationship:

$$\mathbf{f} = \mathbf{f}_d - T_d\mathbf{S}^2(\mathbf{r}_3)\,\mathbf{r}_{3d}. \tag{5}$$

The desired thrust direction is thus calculated as

$$\mathbf{r}_{3d} := -1/T_d\mathbf{f}_d. \tag{6}$$

It is important to note that $\mathbf{r}_{3d}$ cannot be chosen arbitrarily. Instead, its selection is always dependent on the desired stabilizing force $\mathbf{f}_d$.

Assumption 1. *The external disturbance $\mathbf{d}$ is continuous, differentiable and bounded.*

Remark 1. *We assume that the external disturbance $\mathbf{d}$ affecting the quadrotor UAVs is continuous, differentiable, and bounded. This assumption is practical and easily met in real-world situations. In general, the external disturbances often exhibit characteristics of having low variability and being persistent, such as in the case of wind, among others. Nevertheless, as stated in references [37], [38], these external disturbances are considered to be vanishing, a perspective that contrasts with the assumption made in our design.*

Lemma 1. *[39] Suppose that a system output $y(t)$ ($y(t) = x_1(t)$) and its n-order derivative are bounded, we consider the following linear system:*

$$\epsilon\dot{\pi}_i = \pi_{i+1},\ i = 1,\ldots,n-1, \tag{7}$$

$$\epsilon\dot{\pi}_n = -\lambda_1\pi_n - \lambda_2\pi_{n-1} - \ldots - \lambda_{n-1}\pi_2 - \pi_1 + x_1(t), \tag{8}$$

where ϵ is any small positive constant, and the parameters $\lambda_1,\ldots,\lambda_{n-1}$ are properly selected such that the polynomial $s^n + \lambda_1 s^{n-1} + \ldots + \lambda_{n-1}s + 1$ is Hurwitz. Then, the following property holds:

$$\xi_k = \frac{\pi_k}{\epsilon^{k-1}} - x_1^{(k-1)} = \epsilon\phi^{(k)},\ k = 1,\ldots,n-1, \tag{9}$$

where $\phi = \pi_n + \lambda_1\pi_{n-1} + \ldots + \lambda_{n-1}\pi_1$ with $\phi^{(k)}$ being the k-order derivative of ϕ. In addition, there exist positive constants $\bar{\xi}_k$ and t^* such that $|\xi_k| \le \bar{\xi}_k$ holds for $\forall t \ge t^*$.

Lemma 2. *[40] Consider the continuous and differentiable bounded function $\phi(t)$, for $t_0 < t < t_1$, if $|\phi(t)|$ satisfies $|\dot{\phi}(t)| \le \delta$ with the positive constant δ, then $\phi(t)$ is bounded.*

Remark 2. *The linear system in* **Lemma 1** *can serve as a state observer to estimate the unknown signals $x_1^{(k-1)}$, $k = 2,\ldots,n-1$, and due to this merit, the linear system will be used in the following design to estimate the derivative of the desired trajectory.* **Lemma 2** *will be employed in the design of observers responsible for estimating the disturbance $\mathbf{d}$.*

B. Fuzzy Logic Systems

Fuzzy logic systems (FLSs) are divided into four components: 1) the knowledge base, which stores information; 2) the fuzzifier, which converts crisp inputs into fuzzy sets; 3) the fuzzy inference engine, which processes fuzzy rules; and 4) the defuzzifier, which converts the fuzzy output into a crisp result.

In this paper, the fuzzy logic system consists of a set of l fuzzy IF-THEN rules, where each rule specifies conditions based on linguistic variables associated with inputs $\mathbf{Z} = [z_1,\ldots,z_n]^\mathsf{T} \in \mathbb{R}^n$ and results in an output linguistic variable $y \in \mathbb{R}$. In this paper, the fuzzy logic system is

$$y(x) = \frac{\sum_{k=1}^{l} y_k \left[\Pi_{i=1}^{n} u_{A_i^k}(z_i)\right]}{\sum_{k=1}^{l} \left[\Pi_{i=1}^{n} u_{A_i^k}(z_i)\right]}, \tag{10}$$

where $u_{A_i^k}(z_i)$ is the membership function which is selected as the Gaussian function defined as

$$u_{A_i^k}(z_i) = \exp\left[-\frac{(z_i - c_{ik})^2}{\xi_{ik}^2}\right], \tag{11}$$

where c_{ik}, $\xi_{ik} > 0$. To provide clarity, let us define the weight vector and fuzzy basis function vector as $\boldsymbol{\Theta} = [y_1, \ldots, y_l]^{\mathsf{T}} \in \mathbb{R}^l$ and $\boldsymbol{\varpi}(\mathbf{Z}) = [\varpi_1(\mathbf{Z}), \ldots, \varpi_l(\mathbf{Z})]^{\mathsf{T}} \in \mathbb{R}^l$ with

$$\varpi_k(\mathbf{Z}) = \frac{\Pi_{i=1}^{n} u_{A_i^k}(z_i)}{\sum_{k=1}^{l}\left[\Pi_{i=1}^{n} u_{A_i^k}(z_i)\right]}, \quad k = 1, \ldots, l. \tag{12}$$

Hence, (10) is written as

$$y(x) = \boldsymbol{\Theta}^{\mathsf{T}} \boldsymbol{\varpi}(\mathbf{Z}). \tag{13}$$

Lemma 3. *For any continuous function $f(\mathbf{Z})$ that operates within a specific, well-defined region $\boldsymbol{\Upsilon}$, there exists a fuzzy logic system described by (13) such that $\sup_{\mathbf{Z}\in\boldsymbol{\Upsilon}} |f(\mathbf{Z}) - \boldsymbol{\Theta}^{\mathsf{T}}\boldsymbol{\varpi}(\mathbf{Z})| \leq \varepsilon$, with any small constant $\varepsilon > 0$.*

FLSs and neural networks are powerful tools for handling model uncertainty [15], [41]. However, in contrast to neural networks, FLSs not only exhibit online self-studying capabilities, but also incorporate expert experience to enhance control effectiveness. Motivated by this, the paper will further explore the use of FLSs to address uncertainties associated with the quadrotor UAVs models.

C. Control Objective

Let $\mathbf{p}_d \in \mathbb{R}^3$ be a curve of class at least $\mathcal{C}^1$ whose time derivatives are bounded. Hence, given a reference trajectory $\mathbf{p}_d$, the objective of this paper is to design a control scheme driving the vehicle's position $\mathbf{p}$ to accurately track the reference trajectory $\mathbf{p}_d$, in the existence of model uncertainty and even external time-varying (non-vanishing) disturbances.

Assumption 2. *[19] The reference trajectory $\mathbf{p}_d$ and its first-order derivative $\dot{\mathbf{p}}_d$ are continuous and bounded.*

IV. Control Design

Before designing controllers in detail, the tracking errors $\mathbf{e_p}$ and $\mathbf{e_v}$ are defined as

$$\mathbf{e_p} = \mathbf{p} - \mathbf{p}_d \in \mathbb{R}^3, \tag{14}$$

$$\mathbf{e_v} = \mathbf{v} - \boldsymbol{\alpha} \in \mathbb{R}^3, \tag{15}$$

where $\mathbf{p}_d \in \mathbb{R}^3$ is the reference trajectory, $\boldsymbol{\alpha} \in \mathbb{R}^3$ is the output of a first-order filter defined later.

A. Position Control

According to (1a), (14) and (15), the derivative of $\mathbf{e_p}$ with respect to (w.r.t.) time yields

$$\dot{\mathbf{e}}_\mathbf{p} = \mathbf{e_v} + \boldsymbol{\alpha} - \dot{\mathbf{p}}_d, \tag{16}$$

where $\boldsymbol{\alpha}$ is governed by the first-order filter defined as

$$\boldsymbol{\zeta}_\mathbf{p}\dot{\boldsymbol{\alpha}} + \boldsymbol{\alpha} = \bar{\boldsymbol{\alpha}}, \tag{17}$$

where $\boldsymbol{\zeta}_\mathbf{p} \in \mathbb{R}^3$ is a positive-definite gain matrix, and $\bar{\boldsymbol{\alpha}} \in \mathbb{R}^3$ is a virtual controller. Building upon (17), let us define the filter error as $\mathbf{y_p} = \boldsymbol{\alpha} - \bar{\boldsymbol{\alpha}}$, leading to $\boldsymbol{\alpha} = \mathbf{y_p} + \bar{\boldsymbol{\alpha}}$. As a result, using the above filter error, (16) is written as

$$\dot{\mathbf{e}}_\mathbf{p} = \mathbf{e_v} + \mathbf{y_p} + \bar{\boldsymbol{\alpha}} - \dot{\mathbf{p}}_d, \tag{18}$$

where the virtual controller $\bar{\boldsymbol{\alpha}}$ is designed as

$$\bar{\boldsymbol{\alpha}} = -\mathbf{K}_1\mathbf{e_p} + \hat{\dot{\mathbf{p}}}_d, \tag{19}$$

where $\mathbf{K}_1 \in \mathbb{R}^{3\times3}$ is a positive-definite symmetric matrix, and $\hat{\dot{\mathbf{p}}}_d \in \mathbb{R}^3$ denotes the estimate of $\dot{\mathbf{p}}_d$ and is defined as $\hat{\dot{\mathbf{p}}}_d = \frac{\boldsymbol{\pi}_2}{\epsilon}$, with $\boldsymbol{\pi}_2$ and ϵ satisfying the following linear system

$$\begin{cases} \epsilon\dot{\boldsymbol{\pi}}_1 = \boldsymbol{\pi}_2, & \text{(20a)} \\ \epsilon\dot{\boldsymbol{\pi}}_2 = -\lambda_1\boldsymbol{\pi}_2 - \boldsymbol{\pi}_1 + \mathbf{p}_d, & \text{(20b)} \end{cases}$$

where ϵ is a positive constant. In fact, the size of the estimate error $\mathbf{h} := \hat{\dot{\mathbf{p}}}_d - \dot{\mathbf{p}}_d \in \mathbb{R}^3$ depends on the constant ϵ, and a small ϵ renders the error $\mathbf{h}$ smaller. According to **Assumption 2**, it is found that $\mathbf{p}_d$ and $\dot{\mathbf{p}}_d$ are continuous and bounded, which implies the linear system described by (20) is also continuous, and therefore $\hat{\dot{\mathbf{p}}}_d$ ($\hat{\dot{\mathbf{p}}}_d = \frac{\boldsymbol{\pi}_2}{\epsilon}$) in (19) is also continuous.

Remark 3. *For practical application, this paper specifically considers scenarios where the desired trajectory $\mathbf{p}_d$ is not predetermined but can be determined in real-time at each time step. According to [42], an illustrative example involves a quadrotor tracking a mobile target, with the target's position continuously updated by a measurement device. To elaborate further, $\mathbf{p}_d$ is obtained in real-time, but its derivative $\dot{\mathbf{p}}_d$ is not known. To address this challenge, the paper introduces a high-gain observer, described by (20), which is used to estimate the unknown desired velocity $\dot{\mathbf{p}}_d$. This means that the proposed method only requires the collection of position information from the desired trajectory $\mathbf{p}_d$ to make accurate tracking.*

The time derivative of $\mathbf{e_v}$ in (15), using (1b), yields

$$m\dot{\mathbf{e}}_\mathbf{v} = \mathbf{f} + m(g\mathbf{e}_3 - \dot{\boldsymbol{\alpha}}) + m\mathbf{d}. \tag{21}$$

In practice, it is difficult or even impossible to obtain accurate mass of a quadrotor, and hence it is assumed that the mass of the quadrotor, m, is unknown. In order to further implement the backstepping design, the actual mass m is separated as nominal parts denoted by m_o and unknown parts denoted by Δm, i.e., $m = m_o + \Delta m$. Utilizing this separation, (21) is written as

$$m_o\dot{\mathbf{e}}_\mathbf{v} = \mathbf{f} + m_o(g\mathbf{e}_3 - \dot{\boldsymbol{\alpha}}) + \Delta m\left(g\mathbf{e}_3 - \dot{\boldsymbol{\alpha}} - \dot{\mathbf{e}}_\mathbf{v}\right) + m\mathbf{d}. \tag{22}$$

Note that the term $\Delta m\left(g\mathbf{e}_3 - \dot{\boldsymbol{\alpha}} - \dot{\mathbf{e}}_\mathbf{v}\right)$ in (22) depends on the unknown part Δm and is thus unavailable. To address this challenge, FLSs are introduced to approximate model uncertainty. Fuzzy approximation is given in the form of

$$\boldsymbol{\Theta}^{\mathsf{T}}\boldsymbol{\varpi}(\mathbf{Z}) = \Delta m\left(g\mathbf{e}_3 - \dot{\boldsymbol{\alpha}} - \dot{\mathbf{e}}_\mathbf{v}\right) + \boldsymbol{\Delta\epsilon}, \tag{23}$$

where $\boldsymbol{\Theta} = \text{blkdiag}\left[\boldsymbol{\Theta}_1, \boldsymbol{\Theta}_2, \boldsymbol{\Theta}_3\right] \in \mathbb{R}^{l\times3}$ denotes the desired weight matrix, $\boldsymbol{\varpi}(\mathbf{Z}) \in \mathbb{R}^l$ denotes the fuzzy membership function, with l being the number of fuzzy sets, $\mathbf{Z} = \left[\mathbf{e}_\mathbf{p}^{\mathsf{T}}, \mathbf{e}_\mathbf{v}^{\mathsf{T}}, g\mathbf{e}_3^{\mathsf{T}}\right]^{\mathsf{T}} \in \mathbb{R}^9$, and $\boldsymbol{\Delta\epsilon}$ is the approximation error that is assumed to be bounded, i.e., there exists a positive constant $\bar{\epsilon}$ such that $\|\boldsymbol{\Delta\epsilon}\| \leq \bar{\epsilon}$.

Using fuzzy approximation in (23), (22) is written as

$$m_o\dot{\mathbf{e}}_\mathbf{v} = \mathbf{f} + m_o(g\mathbf{e}_3 - \dot{\boldsymbol{\alpha}}) + \boldsymbol{\Theta}^{\mathsf{T}}\boldsymbol{\varpi}(\mathbf{Z}) + \boldsymbol{\mathcal{D}}, \tag{24}$$

where $\boldsymbol{\mathcal{D}} = m\mathbf{d} - \boldsymbol{\Delta}\epsilon \in \mathbb{R}^3$. To mitigate the influence of both the external disturbance $\mathbf{d}$ and the approximation error $\boldsymbol{\Delta}\epsilon$, a disturbance observer will be designed. First, the auxiliary variable $\boldsymbol{\eta} \in \mathbb{R}^3$ is defined as

$$\boldsymbol{\eta} = \boldsymbol{\mathcal{D}} - \boldsymbol{\Phi}\left(\mathbf{e_v}\right) \in \mathbb{R}^3, \tag{25}$$

where $\boldsymbol{\Phi}\left(\mathbf{e_v}\right) : \mathbb{R}^3 \to \mathbb{R}^3$ is a nonlinear function vector. The derivative of $\boldsymbol{\eta}$ in (25) w.r.t. time, using (24), yields

$$\dot{\boldsymbol{\eta}} = \dot{\boldsymbol{\mathcal{D}}} - \frac{1}{m_o}\mathbf{K}_{\boldsymbol{\eta}}\left(\mathbf{f} + m_o(g\mathbf{e}_3 - \dot{\boldsymbol{\alpha}}) + \boldsymbol{\Theta}^{\mathsf{T}}\boldsymbol{\varpi}(\mathbf{Z}) + \boldsymbol{\mathcal{D}}\right), \tag{26}$$

where $\mathbf{K}_{\boldsymbol{\eta}} = \frac{d\boldsymbol{\Phi}(\mathbf{e_v})}{d\mathbf{e_v}^{\mathsf{T}}} \in \mathbb{R}^{3\times 3}$. For simplification and implementation, it is general to choose $\boldsymbol{\Phi}\left(\mathbf{e_v}\right)$ as a linear function of $\mathbf{e_v}$ such that $\mathbf{K}_{\boldsymbol{\eta}}$ is a constant matrix.

Define $\hat{\boldsymbol{\eta}} \in \mathbb{R}^3$ as the estimate of $\boldsymbol{\eta}$, and the dynamics of $\hat{\boldsymbol{\eta}}$ is designed as

$$\dot{\hat{\boldsymbol{\eta}}} = -\frac{1}{m_o}\mathbf{K}_{\boldsymbol{\eta}}\left(\mathbf{f} + m_o(g\mathbf{e}_3 - \dot{\boldsymbol{\alpha}}) + \hat{\boldsymbol{\Theta}}^{\mathsf{T}}\boldsymbol{\varpi}(\mathbf{Z}) + \hat{\boldsymbol{\mathcal{D}}}\right), \tag{27}$$

where $\hat{\boldsymbol{\Theta}}$ and $\hat{\boldsymbol{\mathcal{D}}}$ are the estimates of $\boldsymbol{\Theta}$ and $\boldsymbol{\mathcal{D}}$, respectively. Now, it is ready to design a disturbance observer defined as

$$\hat{\boldsymbol{\mathcal{D}}} = \hat{\boldsymbol{\eta}} + \mathbf{K}_{\boldsymbol{\eta}}\mathbf{e_v}. \tag{28}$$

Then, the observer error $\widetilde{\boldsymbol{\mathcal{D}}} \in \mathbb{R}^3$ is defined as $\widetilde{\boldsymbol{\mathcal{D}}} = \hat{\boldsymbol{\mathcal{D}}} - \boldsymbol{\mathcal{D}}$. By using (25) and (28), it follows that $\dot{\widetilde{\boldsymbol{\mathcal{D}}}} = \dot{\hat{\boldsymbol{\mathcal{D}}}} - \dot{\boldsymbol{\mathcal{D}}} \implies \dot{\widetilde{\boldsymbol{\mathcal{D}}}} = \dot{\hat{\boldsymbol{\eta}}} - \dot{\boldsymbol{\eta}}$. Utilizing (26) and (27), we have

$$\dot{\widetilde{\boldsymbol{\mathcal{D}}}} = -\dot{\boldsymbol{\mathcal{D}}} - \frac{1}{m_o}\mathbf{K}_{\boldsymbol{\eta}}\left(\widetilde{\boldsymbol{\Theta}}^{\mathsf{T}}\boldsymbol{\varpi}\left(\mathbf{Z}\right) + \widetilde{\boldsymbol{\mathcal{D}}}\right). \tag{29}$$

Substituting (5) into (24) yields

$$\begin{aligned} m_o\dot{\mathbf{e}}_{\mathbf{v}} =& \mathbf{f}_d - T_d\mathbf{S}^2(\mathbf{r}_3)\,\mathbf{r}_{3d} + m_o(g\mathbf{e}_3 - \dot{\boldsymbol{\alpha}}) \\ &+ \boldsymbol{\Theta}^{\mathsf{T}}\boldsymbol{\varpi}(\mathbf{Z}) + \boldsymbol{\mathcal{D}}, \end{aligned} \tag{30}$$

where the desired stabilization force $\mathbf{f}_d$ is obtained from a first-order filter defined as

$$\boldsymbol{\zeta}_{\mathbf{v}}\dot{\bar{\mathbf{f}}}_d + \mathbf{f}_d = \bar{\mathbf{f}}_d, \tag{31}$$

where $\boldsymbol{\zeta}_{\mathbf{v}} \in \mathbb{R}^{3\times 3}$ is a positive-definite gain matrix, and $\bar{\mathbf{f}}_d \in \mathbb{R}^3$ is an intermediate stabilization force. Define the error of the filter (31) as $\mathbf{y_f} = \mathbf{f}_d - \bar{\mathbf{f}}_d \implies \mathbf{f}_d = \mathbf{y_f} + \bar{\mathbf{f}}_d$. Using the transformation, (30) is written as

$$\begin{aligned} m_o\dot{\mathbf{e}}_{\mathbf{v}} =& \bar{\mathbf{f}}_d + \mathbf{y_f} - T_d\mathbf{S}^2(\mathbf{r}_3)\,\mathbf{r}_{3d} + m_o(g\mathbf{e}_3 - \dot{\boldsymbol{\alpha}}) \\ &+ \boldsymbol{\Theta}^{\mathsf{T}}\boldsymbol{\varpi}(\mathbf{Z}) + \boldsymbol{\mathcal{D}}. \end{aligned} \tag{32}$$

The intermediate stabilization force $\bar{\mathbf{f}}_d$ is designed as

$$\bar{\mathbf{f}}_d = -\mathbf{K}_2\mathbf{e_v} - \mathbf{e_p} - m_o\left(g\mathbf{e}_3 - \dot{\boldsymbol{\alpha}}\right) - \hat{\boldsymbol{\Theta}}^{\mathsf{T}}\boldsymbol{\varpi}(\mathbf{Z}) - \hat{\boldsymbol{\mathcal{D}}}, \tag{33}$$

where $\mathbf{K}_2 \in \mathbb{R}^{3\times 3}$ is a positive-definite symmetric matrix, $\hat{\mathcal{D}}$ is obtained from the observer (28), and the adaptation law for the weight $\hat{\boldsymbol{\Theta}}$ is designed as

$$\dot{\hat{\boldsymbol{\Theta}}}_i = -\boldsymbol{\Gamma}\left(\boldsymbol{\varpi}(\mathbf{Z})\mathbf{e}_{\mathbf{v},i} + \sigma\hat{\boldsymbol{\Theta}}_i\right), \; i = 1, 2, 3, \tag{34}$$

where $\boldsymbol{\Gamma} \in \mathbb{R}^{l\times l}$ is a positive-definite symmetric matrix, and σ is a positive constant that is used to enhance robustness under disturbances.

Up to this point, we have finalized the design of the intermediate desired stabilization force $\bar{\mathbf{f}}_d$ to achieve position control for the quadrotor. Subsequently, the primary focus in the next design phase is to stabilize the attitude subsystem, aiming to compel the vehicle to generate the specified force $\bar{\mathbf{f}}_d$ described by (33).

Remark 4. *Adaptive techniques are effective tools for addressing model uncertainty and automatically adjusting system behavior [43]. Motivated by this, we design the adaption law $\dot{\hat{\boldsymbol{\Theta}}}_i, i = 1, 2, 3$, as displayed in (34) to automatically adjust the weight of FLSs for approximating the unknown part of the quadrotor's mass, Δm. In addition, $\hat{\boldsymbol{\eta}}$ is also adaptively changed according to its dynamics, as designed in (27), such that the disturbance observer $\hat{\boldsymbol{\mathcal{D}}}$, as shown in (28), is synthetized to compensate the external disturbance $\mathbf{d}$ and the approximation error $\boldsymbol{\Delta}\boldsymbol{\epsilon}$.*

B. Attitude Control

To stabilize the attitude subsystem, according to the desired thrust direction $\mathbf{r}_{3d}$ defined in (6) and the actual thrust direction $\mathbf{r}_3$ defined in (3), we define the attitude error as

$$\mathbf{e_r} = \mathbf{r}_3 - \mathbf{r}_{3d} \in \mathbb{R}^3. \tag{35}$$

Inspired by the idea of triggered threshold strategy in [44], we design an event-triggered rule with a time-varying threshold which depends on the tracking errors of the closed-loop system. Let the angular velocity $\boldsymbol{\Omega}$ be synthesized according to an event-triggered mechanism defined as

$$\begin{cases} \boldsymbol{\Omega}\left(t\right) = \hat{\boldsymbol{\Omega}}\left(t_k\right), \; \forall t \in [t_k, t_{k+1}), & \text{(36a)} \\ t_{k+1} = \inf\{t > t_k |\; \mathbf{b}^{\mathsf{T}}\mathbf{b}(\vartheta_1\mathbf{e_p}^{\mathsf{T}}\mathbf{e_p} + \vartheta_2\mathbf{e_v}^{\mathsf{T}}\mathbf{e_v} \\ \qquad + \vartheta_3\|\mathbf{S}(\mathbf{r}_3)\,\mathbf{r}_{3d}\|^2 + y) \geq 1\}, & \text{(36b)} \end{cases}$$

where $\hat{\boldsymbol{\Omega}}$ is the intermediate angular velocity to be designed later, ϑ_i, $i = 1, 2, 3$, and y are positive constants, $\mathbf{b} = \boldsymbol{\Omega} - \hat{\boldsymbol{\Omega}}$ is the measure input error, t_k with $k \in \mathbf{z}^+$ is the controller update time. It is found from (36) that when the above triggering condition is satisfied, the angular velocity $\boldsymbol{\Omega}(t)$ will be updated to $\hat{\boldsymbol{\Omega}}(t_{k+1})$, and otherwise, it will keep a constant, i.e., $\boldsymbol{\Omega}(t) = \hat{\boldsymbol{\Omega}}(t_k)$. Then, the intermediate angular velocity $\hat{\boldsymbol{\Omega}}$ is designed as

$$\begin{aligned} \hat{\boldsymbol{\Omega}} = -\,&\mathbf{S}^2(\mathbf{e}_3)\left[\mathbf{R}^{\mathsf{T}}\mathbf{S}(\mathbf{r}_{3d})\,\dot{\mathbf{r}}_{3d} + \frac{w_{\mathbf{r}}}{k_{\mathbf{r}}}\mathbf{S}(\mathbf{e}_3)\,\mathbf{R}^{\mathsf{T}}\mathbf{r}_{3d}\right. \\ &\left. + \frac{T_d}{k_{\mathbf{r}}}\mathbf{S}(\mathbf{e}_3)\,\mathbf{R}^{\mathsf{T}}\mathbf{e_v}\right] + \hat{\Omega}_3\mathbf{e}_3, \end{aligned} \tag{37}$$

where, $w_{\mathbf{r}}$ and $k_{\mathbf{r}}$ stand for positive constants. Additionally, $\hat{\Omega}_3 : \mathbb{R} \to \mathbb{R}$ denotes an arbitrary time-dependent function representing the third component of the vector $\hat{\boldsymbol{\Omega}}$. The term $\hat{\Omega}_3\mathbf{e}_3$ can be applied, for instance, to modify the vehicle's yaw using a proportional control law.

The development of the observer-based fuzzy event-triggered control algorithm is now complete, as depicted in Fig. 1. Detailed results regarding the proposed algorithm will be provided in the following theorem.

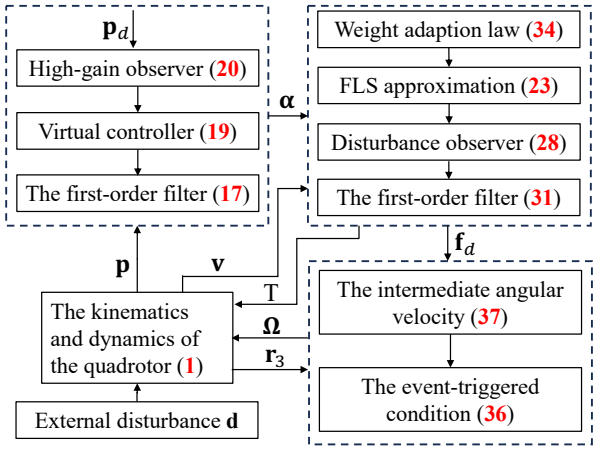

Figure 1. The observer-based fuzzy event-triggered control scheme.

Theorem 1. *For the unmanned aerial vehicle system described by (1), coupled with the disturbance observer in (28), under the action of the event-triggered control scheme (36) as well as the intermediate desired angular velocity (37), with* $\mathbf{f}$ *and* $\bar{\mathbf{f}}_d$ *given in (5) and (33), respectively, given some positive number* p_l*, for all initial conditions satisfying* $2V_3 \leq p_l$*, the errors* $\mathbf{e_p}$*,* $\mathbf{e_v}$*,* $\widetilde{\boldsymbol{\Theta}}_i$*,* $i = 1, 2, 3$*,* $\widetilde{\boldsymbol{\mathcal{D}}}$*,* $\mathbf{y_p}$*,* $\mathbf{y_f}$ *and* $\mathbf{e_r}$ *are uniformly ultimately bounded (UUB), where* $V_3 = \frac{1}{2}\mathbf{e_p}^{\mathsf{T}}\mathbf{e_p} + \frac{1}{2}\mathbf{y_p}^{\mathsf{T}}\mathbf{y_p} + \frac{m_o}{2}\mathbf{e_v}^{\mathsf{T}}\mathbf{e_v} + \frac{1}{2}\sum_{i=1}^{3}\widetilde{\boldsymbol{\Theta}}_i^{\mathsf{T}}\boldsymbol{\Gamma}^{-1}\widetilde{\boldsymbol{\Theta}}_i + \frac{1}{2}\widetilde{\boldsymbol{\mathcal{D}}}^{\mathsf{T}}\widetilde{\boldsymbol{\mathcal{D}}} + \frac{1}{2}\mathbf{y_f}^{\mathsf{T}}\mathbf{y_f} + \frac{k_r}{2}\mathbf{e_r}^{\mathsf{T}}\mathbf{e_r}$.

Proof. Please refer to Appendix. □

According to **Theorem 1**, it is obtained that $\mathbf{e_p}$, $\mathbf{e_v}$, $\widetilde{\boldsymbol{\Theta}}_i$, $i = 1, 2, 3$, $\widetilde{\boldsymbol{\mathcal{D}}}$, $\mathbf{y_p}$, $\mathbf{y_f}$ and $\mathbf{e_r}$ are bounded. According to **Assumption 2**, $\mathbf{p}_d$ is bounded, and with the help of the high-gain observer (20), it follows that $\hat{\mathbf{p}}_d$ is bounded. Hence, $\bar{\boldsymbol{\alpha}}$ in (19) is bounded. The intermediate stabilization force $\bar{\mathbf{f}}_d$ in (33) is a function of the above bounded variables, and therefore also bounded. According to the first-order filter, we have that the desired stabilization force $\mathbf{f}_d$ in (31) is bounded. The intermediate angular velocity $\hat{\boldsymbol{\Omega}}$ in (37) is a function of the above bounded variables, and therefore also bounded. With the aid of **Lemma 2**, it follows that $\dot{\hat{\boldsymbol{\Omega}}}$ is bounded. As a result, There exist a positive constants c such that $\|\dot{\hat{\boldsymbol{\Omega}}}\| \leq c$.

Now, let us discuss the Zeno behavior of the event-triggered mechanism (36). According to the triggering condition given in (36), $\boldsymbol{\Omega}(t)$ will be updated to $\hat{\boldsymbol{\Omega}}(t_k)$ if and only if $\mathbf{b}^{\mathsf{T}}\mathbf{b}(\vartheta_1\mathbf{e_p}^{\mathsf{T}}\mathbf{e_p} + \vartheta_2\mathbf{e_v}^{\mathsf{T}}\mathbf{e_v} + \vartheta_3\|\mathbf{S}(\mathbf{r}_3)\,\mathbf{r}_{3d}\|^2 + y) \geq 1$, which implies that $\mathbf{b}^{\mathsf{T}}\mathbf{b}(\vartheta_1\mathbf{e_p}^{\mathsf{T}}\mathbf{e_p} + \vartheta_2\mathbf{e_v}^{\mathsf{T}}\mathbf{e_v} + \vartheta_3\|\mathbf{S}(\mathbf{r}_3)\,\mathbf{r}_{3d}\|^2 + y) \leq 1$ for all $t \geq 0$. Since $\mathbf{b} = \boldsymbol{\Omega} - \hat{\boldsymbol{\Omega}}$ for $\forall t \in [t_k, t_{k+1})$, there exists

$$\frac{d\|\mathbf{b}\|}{dt} = \frac{d\sqrt{\mathbf{b}^{\mathsf{T}}\mathbf{b}}}{dt} = \frac{\mathbf{b}^{\mathsf{T}}\dot{\mathbf{b}}}{\sqrt{\mathbf{b}^{\mathsf{T}}\mathbf{b}}} \leq \frac{\|\mathbf{b}\|\|\dot{\mathbf{b}}\|}{\|\mathbf{b}\|} = \|\dot{\hat{\boldsymbol{\Omega}}}\|. \tag{38}$$

By noting that $\lim_{t\to t_k}\|\mathbf{b}\| = 0$ and $\lim_{t\to t_{k+1}}\|\mathbf{b}\| = \aleph$, where $\aleph = \frac{1}{\sqrt{\vartheta_1\mathbf{e_p}^{\mathsf{T}}\mathbf{e_p} + \vartheta_2\mathbf{e_v}^{\mathsf{T}}\mathbf{e_v} + \vartheta_3\|\mathbf{S}(\mathbf{r}_3)\mathbf{r}_{3d}\|^2 + y}}$, thus there exists a positive constant t^* such that

$$\{t_{k+1} - t_k\} \geq t^* \geq \frac{\aleph}{\|\dot{\hat{\boldsymbol{\Omega}}}\|} \geq \frac{\aleph}{c} > 0, \tag{39}$$

which implies that the Zeno behavior is ruled out.

Remark 5. *In [23], [45], fixed threshold and relative threshold strategies are proposed for event-triggered control of uncertain nonlinear systems. In [46], a novel dynamic event-triggered mechanism is designed to effectively reduce the signal transmission frequency. However, establishing a direct, explicit relationship between the triggering thresholds and the tracking error of the controlled system is challenging. To address this, the paper introduces a time-varying triggering threshold linked to the tracking error, as defined by (36b). More specifically, it is evident from (39) that 1) when the errors* $\mathbf{e_p}$*,* $\mathbf{e_v}$*, and* $\|\mathbf{S}(\mathbf{r}_3)\,\mathbf{r}_{3d}\|$ *become large,* $\aleph$ *will decrease, which implies that a smaller threshold makes more precise control applied to the system such that better system performance can be obtained; and 2) when the errors* $\mathbf{e_p}$*,* $\mathbf{e_v}$*, and* $\|\mathbf{S}(\mathbf{r}_3)\,\mathbf{r}_{3d}\|$ *are very small,* $\aleph$ *will increase, which implies that the consecutive time interval between two events will increase, and thus longer update intervals are obtained. In this way, the number of the triggered events will be decreased effectively, while still remaining accurate tracking.*

Remark 6. *The parameters* ϑ_i*,* $i = 1, 2, 3$ *and* y *in (36b) are crucial for reducing the number of triggered events. However, it is worth noting that a decrease in triggered events generally comes at the expense of accuracy. Therefore, there exists a trade-off between the tracking control accuracy and the number of triggered events. In addition, when* $\vartheta_i = 0$*,* $i = 1, 2, 3$*, the triggering mechanism (36b) will degenerate to the fixed threshold approach in [23].*

Remark 7. *The dynamic surface control (DSC) technique has proven effective in mitigating the computational load resulting from the repeated differentiation of the virtual control in iterative backstepping designs [47]. Notably, this approach employs the first-order filters, as shown in (17) and (31), for the design of the virtual controllers* $\bar{\boldsymbol{\alpha}}$ *and* $\bar{\mathbf{f}}_\mathbf{d}$*. Note that the matrices* $\boldsymbol{\zeta}_\mathbf{p}$ *and* $\boldsymbol{\zeta}_\mathbf{v}$ *in (17) and (31) act as cut-off frequencies, which can be tuned in practice. In* **Theorem 1***, the quadrotor's initial values must adhere to the condition* $2V_3 \leq p_l$*. Nevertheless, given the allowance for* p_l *to be arbitrarily large, this condition does not pose significant restrictions, which is consistent with the result in [47].*

Remark 8. *This paper utilizes the disturbance observer (28) to estimate the composite disturbance* $\boldsymbol{\mathcal{D}}$ *(*$\boldsymbol{\mathcal{D}} = m\mathbf{d} - \boldsymbol{\Delta}\epsilon$*). As stated in the proof of* **Theorem 1***, the derivative of the composite disturbance* $\boldsymbol{\mathcal{D}}$ *is shown to be only bounded, which implies that the disturbance can be non-vanishing.*

V. Simulation Results

In this section, some examples will be used to verify the effectiveness of the proposed method. Consider the reference trajectory $\mathbf{p}_d$ as

$$\mathbf{p}_d := \begin{bmatrix} \sin(t) \\ \cos(t) \\ 2 + 0.5\sin(t) \end{bmatrix} \text{ (m)}. \tag{40}$$

The initial position of the quadrotor is set to $\mathbf{p}(0) = [0\ 0.8\ 2]^{\mathsf{T}}$ (m). The practical constants of the vehicle described by (1) are $m = 0.53$ kg and $g = 9.81$ m/s^2. The

initial conditions of $\boldsymbol{\pi}_1$ and $\boldsymbol{\pi}_2$, as given by the linear system (20), are set to $\boldsymbol{\pi}_1 = [0\ 1\ 2.2]^{\mathsf{T}}$ (m) and $\boldsymbol{\pi}_2 = [0\ 0\ 0]^{\mathsf{T}}$ (m/s). For the FLSs, nine fuzzy sets A_j^i $(i = 1, \ldots, 9; j = 1, \ldots, 9)$ are characterized by the following membership functions:

$$u_{A_i^1}(z_i) = \exp\left[-\frac{(z_i+2)^2}{2}\right], u_{A_i^2}(z_i) = \exp\left[-\frac{(z_i+1.5)^2}{2}\right],$$
$$u_{A_i^3}(z_i) = \exp\left[-\frac{(z_i+1)^2}{2}\right], u_{A_i^4}(z_i) = \exp\left[-\frac{(z_i+0.5)^2}{2}\right],$$
$$u_{A_i^5}(z_i) = \exp\left[-\frac{z_i^2}{2}\right], u_{A_i^6}(z_i) = \exp\left[-\frac{(z_i-0.5)^2}{2}\right],$$
$$u_{A_i^7}(z_i) = \exp\left[-\frac{(z_i-1)^2}{2}\right], u_{A_i^8}(z_i) = \exp\left[-\frac{(z_i-1.5)^2}{2}\right],$$
$$u_{A_i^9}(z_i) = \exp\left[-\frac{(z_i-2)^2}{2}\right].$$

The initial conditions of FLSs weights are set to $\hat{\boldsymbol{\Theta}}_i = \mathbf{0}$, $i = 1, 2, 3$. To fully show the merits of the proposed method, the whole simulation will include two cases. Detailed results are as follows.

A. *Case 1: the external disturbance* $\mathbf{d} = \mathbf{0}$.

This case aims to confirm the effectiveness of the proposed method without the effect of external disturbances. The controller gains and event-triggered condition parameters are provided in Table I. Please note that nominal mass m_o is known to simulation, but actual mass m is unknown. Note that the event-triggered parameters in Table I aim to adjust the triggering threshold, i.e., when $\mathbf{b}^{\mathsf{T}}\mathbf{b}(\vartheta_1 \mathbf{e}_{\mathbf{p}}^{\mathsf{T}}\mathbf{e}_{\mathbf{p}} + \vartheta_2 \mathbf{e}_{\mathbf{v}}^{\mathsf{T}}\mathbf{e}_{\mathbf{v}} + \vartheta_3 \|\mathbf{S}(\mathbf{r}_3)\,\mathbf{r}_{3d}\|^2 + y) \geq 1$, an event will be triggered.

Table I
SYSTEM PARAMETERS - SIMULATION

	Symbol	Value
Control gains	$\mathbf{K}_{\boldsymbol{\eta}}$	$2\mathbf{I}$
	$\mathbf{K}_1$	$\mathrm{diag}(9, 9, 9)$
	$\mathbf{K}_2$	$\mathrm{diag}(2.3, 1.2, 1.4)$
	$\boldsymbol{\zeta}_{\mathbf{p}}, \boldsymbol{\zeta}_{\mathbf{v}}$	$0.02\mathbf{I}, 0.04\mathbf{I}$
	$\omega_{\mathbf{r}}, k_{\mathbf{r}}$	$2, 12$
	$\boldsymbol{\Gamma}, \sigma$	$20\mathbf{I}, 0.6$
	λ_1, ϵ	$1.6, 0.08$
Event-triggered parameters	$\vartheta_1, \vartheta_2, \vartheta_3$	$0.5, 0.7, 0.7$
	y	30

Simulation results are shown in Figs. 2-8. Fig. 2 plots the reference trajectory $\mathbf{p}_d$ and the actual position $\mathbf{p}$ of the quadrotor UAV, respectively, and it is found from this figure that the quadrotor initiates the maneuver relatively far from the reference position and remains close to it even in the presence of model uncertainty caused by the unknown quadrotor mass. As illustrated by Fig. 3, the tracking error $\mathbf{e}_{\mathbf{p}}$ quickly decreases and ultimately converges to a neighborhood of zero, which is definitely consistent with the result provided by Fig. 2. Fig. 4 provides the evolution of the thrust T. In Fig. 5, the angular velocity $\boldsymbol{\Omega}$ is plotted. Fig. 6 gives the evolution of the norm of FLS weights, and from this figure, it is obtained that FLSs adaptively adjust the weight to compensate for the model uncertainty of the vehicle to enhance the tracking accuracy. In Fig. 7, the evolution of the disturbance observer is plotted. Although the external disturbance $\mathbf{d}$ is moved in *Case 1*, due to the unknown approximation error $\boldsymbol{\Delta}\boldsymbol{\epsilon}$ caused by the FLSs, the disturbance observer does not converge to zero, as shown by Fig. 7. From Fig. 8, the event is triggered frequently in the initial stage, because the large initial errors make the triggered threshold become small. However, when the errors are very small, the triggering threshold will become large, which implies that the number of the triggering events are decreased, as presented in Fig. 8.

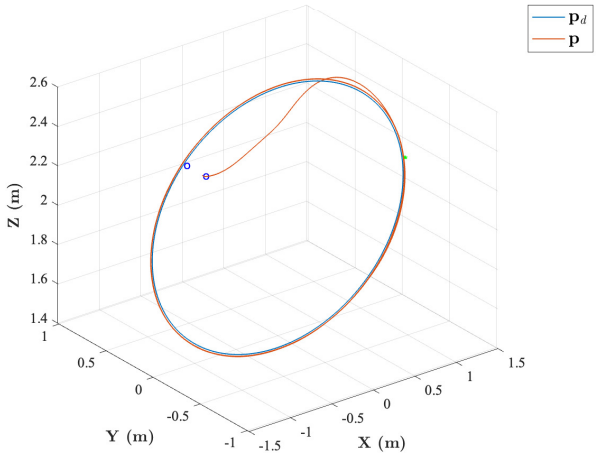

Figure 2. Reference curve $\mathbf{p}_d$ vs. actual position $\mathbf{p}$ of the quadrotor UAV for Case 1. (Circle and star mark denotes the starting and ending positions of each trajectory, respectively.)

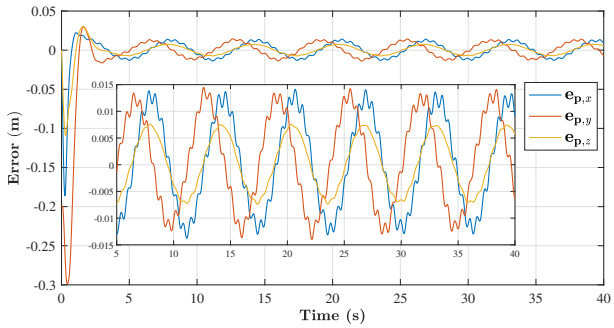

Figure 3. Evolution of the tracking error $\mathbf{e}_{\mathbf{p}}$ for Case 1.

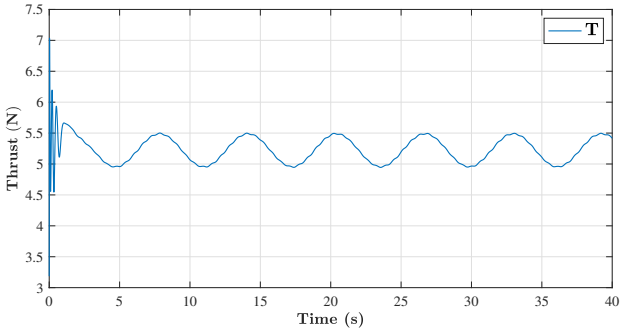

Figure 4. Evolution of the actual thrust T for Case 1.

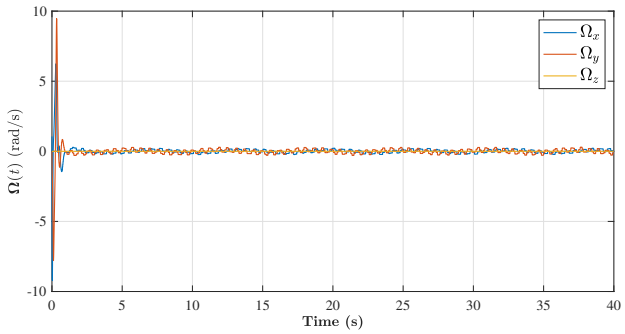

Figure 5. Evolution of the angular velocity $\mathbf{\Omega}$ for Case 1.

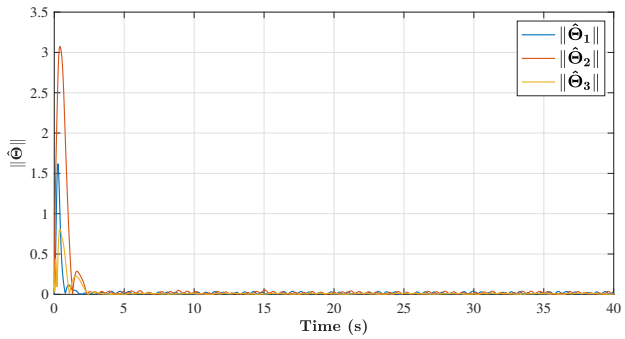

Figure 6. Evolution of the norm of fuzzy system weights for Case 1.

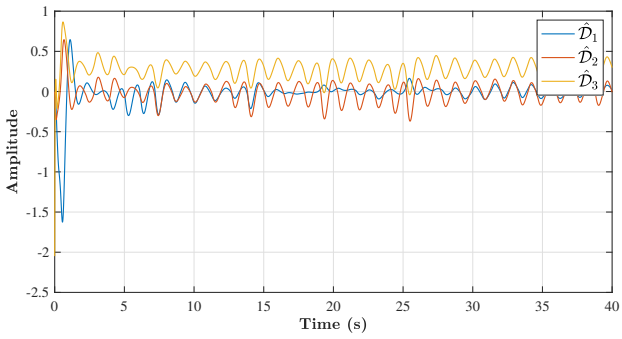

Figure 7. Evolution of the disturbance observer $\hat{\mathcal{D}}$ for Case 1.

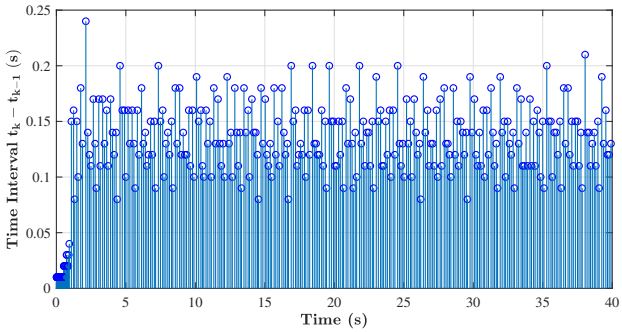

Figure 8. Consecutive time intervals for Case 1.

B. Case 2: the external disturbance $\mathbf{d}$ *is characterized as random signals, as defined in* (41).

This case aims to validate the robustness of the proposed method in the presence of unknown disturbances. The controller gains and event-triggered condition parameters are provided in Table II. For more explanations about gain and parameter choice in Table II, please refer to *Case 1*. Furthermore, in order to obtain more practical results, it is assumed that the vehicle is exposed to a significant source of continuously changing external disturbances following a Brownian motion pattern. To be more precise, these disturbances are not characterized by a regular or repeating pattern, but rather influenced by a factor denoted as

$$\dot{\mathbf{d}} = 10\text{diag}(13.5\ 15\ 14)^{-1}\left[-\mathbf{d} + \text{diag}(8\ 7.5\ 11)\mathbf{wd}\right], \quad (41)$$

where $\mathbf{wd} \in \mathbb{R}^3$ is a vector of zero-mean white Gaussian noise sequences generated from different seeds.

Table II
SYSTEM PARAMETERS - SIMULATION

	Symbol	Value
Control gains	$\mathbf{K}_{\boldsymbol{\eta}}$	$54.9\mathbf{I}$
	$\mathbf{K}_1$	$\text{diag}(8, 9, 9)$
	$\mathbf{K}_2$	$\text{diag}(1.8, 1.6, 0.91)$
	$\boldsymbol{\zeta}_{\mathbf{p}}, \boldsymbol{\zeta}_{\mathbf{v}}$	$0.02\mathbf{I}, 0.04\mathbf{I}$
	$\omega_{\mathbf{r}}, k_{\mathbf{r}}$	$2, 12$
	$\boldsymbol{\Gamma}, \sigma$	$5\mathbf{I}, 0.2$
	λ_1, ϵ	$1.6, 0.08$
Event-triggered parameters	$\vartheta_1, \vartheta_2, \vartheta_3$	$0.5, 0.7, 0.7$
	y	1.3

Simulation results are presented in Figs. 9-15. The reference trajectory $\mathbf{p}_d$ and the actual position trajectory $\mathbf{p}$ are given in Fig. 9, and from this figure, it is found that the quadrotor starts to approach the reference trajectory $\mathbf{p}_d$ from the initial position ($\mathbf{p}(0) = [0\ 0.8\ 2]^{\mathsf{T}}$ (m)) and remains close to it even in the presence of model uncertainty stemming from the unknown quadrotor mass and the time-varying external disturbance $\mathbf{d}$ governed by (41) and plotted by Fig. 14. Due to the FLSs approximating for model uncertainty and the disturbance observer compensation for the external disturbance $\mathbf{d}$, the proposed method will force the quadrotor to accurately track the reference trajectory, with strong robustness, which is also intuitively illustrated by the evolution of the tracking error $\mathbf{e}_{\mathbf{p}}$, as presented by Fig. 10. The thrust T and the angular velocity $\mathbf{\Omega}$ are presented in Figs. 11 and 12, and high-frequent oscillations are observed in $\mathbf{\Omega}$ because the quadrotor UAV needs to adjust its attitude to resist the disturbance. From Fig. 13, it is obtained that the norm $\|\hat{\mathbf{\Theta}}\|$ adaptively evolves in the initial stages of adaptation and ultimately converge to a neighborhood of their true values, which implies an effective compensation for model uncertainty. Finally, the actual disturbance $\boldsymbol{\mathcal{D}}$ and its estimation $\hat{\boldsymbol{\mathcal{D}}}$ are presented in Fig. 14, and from this figure, it is observed that the designed disturbance observer can accurately estimate the disturbance $\boldsymbol{\mathcal{D}}$. From Fig. 15, the event is triggered frequently in the initial stage, because the large initial errors make the triggered threshold become small. However, when the errors are very small, the number of the triggering events is reduced, as presented in Fig. 15.

By examining the aforementioned two cases, it is concluded that despite the partial loss of information regarding the control signal $\mathbf{\Omega}$ caused by the event-triggered mechanism, the introduction of compensation methods, such as FLSs and disturbance observers, not only substantially decreases the frequency of triggering events but also ensures that the quadrotor exhibits satisfactory performance. According to Figs. 3 and

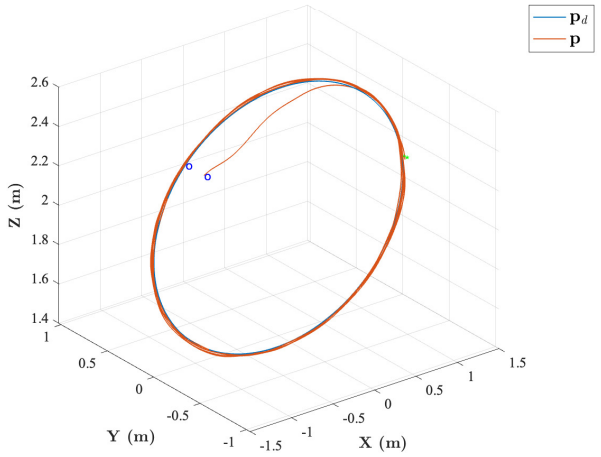

Figure 9. Reference curve $\mathbf{p}_d$ vs. actual position $\mathbf{p}$ of the quadrotor UAV for Case 2. (Circle and star mark denotes the starting and ending positions of each trajectory, respectively.)

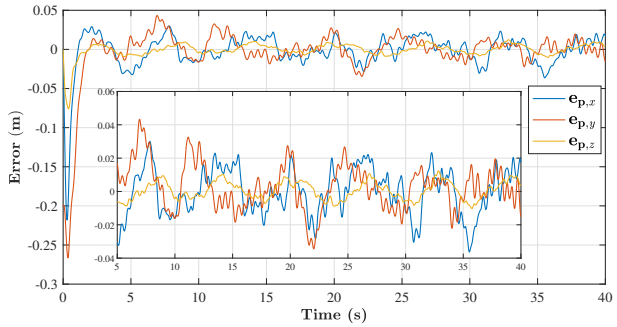

Figure 10. Evolution of the tracking error $\mathbf{e}_\mathbf{p}$ for Case 2.

10, the tracking error $\mathbf{e}_\mathbf{p}$ for *Case 2* is obviously larger than one of *Case 1* because the disturbance $\mathbf{d}$ described in (41) is acted. Additionally, based on Figs. 3 and 10, it is also observed that high-frequency oscillations exist in $\mathbf{e}_\mathbf{p}$. These oscillations can be attributed to: i) rapid unmodeled dynamics and external disturbances that are not entirely compensated for by the FLSs and disturbance observer, respectively; and ii) a lack of compensation for the measurement error $\mathbf{b}$ under the event-triggered condition.

VI. Conclusion

In this paper, we developed an event-triggered control scheme for trajectory tracking of an underactuated autonomous aerial vehicle with model uncertainty, in the presence of unknown non-vanishing disturbances, under the constraint that the derivative of the reference trajectory is not available. A high-gain observer was first introduced to estimate the unknown derivative of the reference trajectory. A disturbance observer was then designed to compensate for the non-vanishing disturbances. FLSs were introduced to address model uncertainty. A new event-triggered mechanism associated with the performance of the closed-loop system was designed. The errors of the closed-loop system were proven to be UUB, which has been verified by simulation results. An intriguing avenue for future research is to propose an optimization scheme using adaptive dynamic programming for the tracking control of underactuated autonomous aerial vehicles in the presence of model uncertainty and unknown disturbances.

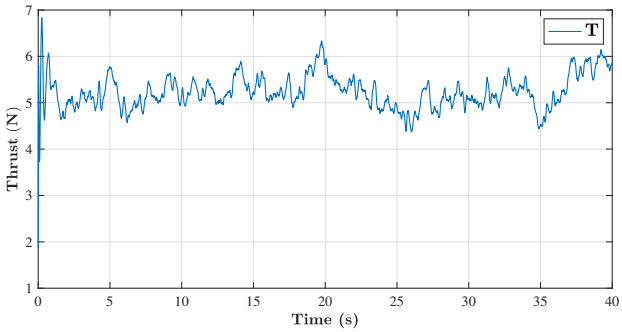

Figure 11. Evolution of the actual thrust T for Case 2.

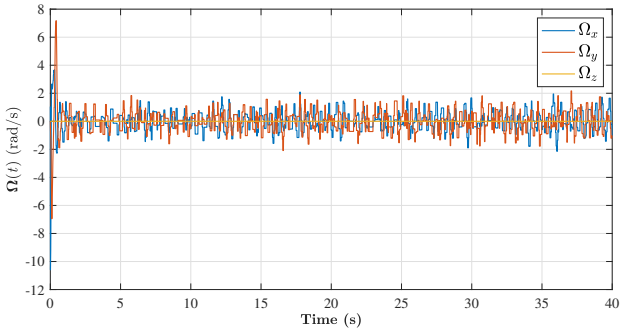

Figure 12. Evolution of the angular velocity $\mathbf{\Omega}$ for Case 2.

Appendix

The proof of Theorem 1 is divided into three parts, which are outlined below.

Part I: Applying the virtual controller $\bar{\boldsymbol{\alpha}}$ given in (19) to (18) yields

$$\dot{\mathbf{e}}_\mathbf{p} = -\mathbf{K}_1\mathbf{e}_\mathbf{p} + \mathbf{e}_\mathbf{v} + \mathbf{h} + \mathbf{y}_\mathbf{p}, \tag{42}$$

where according to **Lemma 1**, $\mathbf{h}$ is bounded such that there exists a positive constant $\bar{h}$ such that $\|\mathbf{h}\| \leq \bar{h}$. Note that the boundedness of $\mathbf{h}$ implies that $\hat{\dot{\mathbf{p}}}_d$ can accurately estimate $\dot{\mathbf{p}}_d$.

Then, to show the boundedness of $\mathbf{e}_\mathbf{p}$, a Lyapunov function candidate is introduced as $V_1 = \frac{1}{2}\mathbf{e}_\mathbf{p}^\mathsf{T}\mathbf{e}_\mathbf{p} + \frac{1}{2}\mathbf{y}_\mathbf{p}^\mathsf{T}\mathbf{y}_\mathbf{p}$, whose derivative w.r.t. time is

$$\dot{V}_1 = -\mathbf{e}_\mathbf{p}^\mathsf{T}\mathbf{K}_1\mathbf{e}_\mathbf{p} + \mathbf{e}_\mathbf{p}^\mathsf{T}(\mathbf{e}_\mathbf{v} + \mathbf{h} + \mathbf{y}_\mathbf{p}) + \mathbf{y}_\mathbf{p}^\mathsf{T}\dot{\mathbf{y}}_\mathbf{p}. \tag{43}$$

Due to the fact that $\mathbf{y}_\mathbf{p} = \boldsymbol{\alpha} - \bar{\boldsymbol{\alpha}}$ and with the help of the filter (17), it follows that $\dot{\mathbf{y}}_\mathbf{p} = \dot{\boldsymbol{\alpha}} - \dot{\bar{\boldsymbol{\alpha}}} \implies \dot{\mathbf{y}}_\mathbf{p} = -\boldsymbol{\zeta}_\mathbf{p}^{-1}\mathbf{y}_\mathbf{p} - \dot{\bar{\boldsymbol{\alpha}}}$. Therefore, (43) is written as

$$\dot{V}_1 = -\mathbf{e}_\mathbf{p}^\mathsf{T}\mathbf{K}_1\mathbf{e}_\mathbf{p} + \mathbf{e}_\mathbf{p}^\mathsf{T}(\mathbf{e}_\mathbf{v} + \mathbf{h} + \mathbf{y}_\mathbf{p}) - \mathbf{y}_\mathbf{p}^\mathsf{T}\left(\boldsymbol{\zeta}_\mathbf{p}^{-1}\mathbf{y}_\mathbf{p} + \dot{\bar{\boldsymbol{\alpha}}}\right). \tag{44}$$

Part II: Applying the intermediate stabilization force $\bar{\mathbf{f}}_d$ in (33) to (32) yields

$$\begin{aligned} m_o\dot{\mathbf{e}}_\mathbf{v} = &-\mathbf{K}_2\mathbf{e}_\mathbf{v} - \mathbf{e}_\mathbf{p} + \widetilde{\mathbf{\Theta}}^\mathsf{T}\boldsymbol{\varpi}(\mathbf{Z}) - \widetilde{\mathcal{D}} \\ &+ \mathbf{y}_\mathbf{f} - T_d\mathbf{S}^2(\mathbf{r}_3)\,\mathbf{r}_{3d}, \end{aligned} \tag{45}$$

where $\widetilde{\mathbf{\Theta}} = \mathbf{\Theta} - \hat{\mathbf{\Theta}}$.

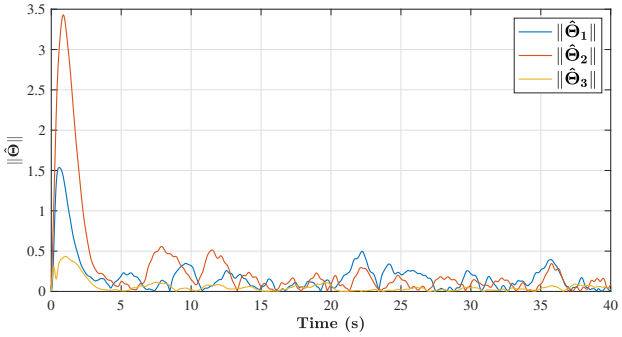

Figure 13. Evolution of the norm of fuzzy system weights for Case 2.

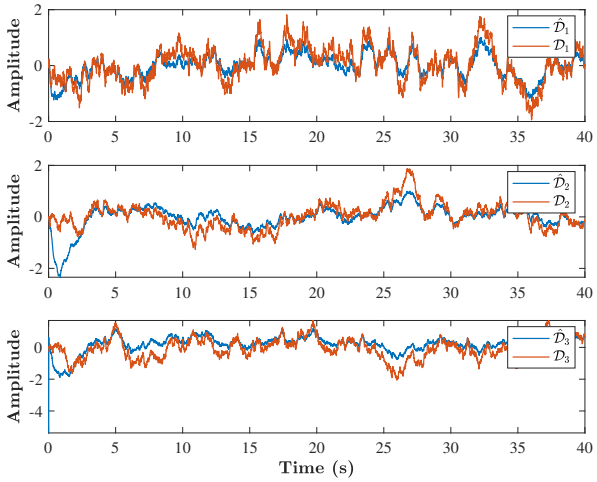

Figure 14. Actual disturbance $\boldsymbol{\mathcal{D}}$ vs. observer estimation $\hat{\boldsymbol{\mathcal{D}}}$ for Case 2.

Then, a Lyapunov function candidate is introduced as

$$V_2 = V_1 + \frac{m_o}{2}\mathbf{e}_\mathbf{v}^\mathsf{T}\mathbf{e}_\mathbf{v} + \frac{1}{2}\sum_{i=1}^{3}\widetilde{\boldsymbol{\Theta}}_i^\mathsf{T}\boldsymbol{\Gamma}^{-1}\widetilde{\boldsymbol{\Theta}}_i + \frac{1}{2}\widetilde{\boldsymbol{\mathcal{D}}}^\mathsf{T}\widetilde{\boldsymbol{\mathcal{D}}} + \frac{1}{2}\mathbf{y}_\mathbf{f}^\mathsf{T}\mathbf{y}_\mathbf{f}, \tag{46}$$

whose derivative w.r.t. time, using (29), (34), (43), and (45), is

$$\begin{aligned}\dot{V}_2 =& -\mathbf{e}_\mathbf{p}^\mathsf{T}\mathbf{K}_1\mathbf{e}_\mathbf{p} - \mathbf{e}_\mathbf{v}^\mathsf{T}\mathbf{K}_2\mathbf{e}_\mathbf{v} - \mathbf{e}_\mathbf{v}^\mathsf{T}T_d\mathbf{S}^2(\mathbf{r}_3)\,\mathbf{r}_{3d} \\ & - \sigma\sum_{i=1}^{3}\widetilde{\boldsymbol{\Theta}}_i^\mathsf{T}\hat{\boldsymbol{\Theta}}_i - \mathbf{e}_\mathbf{v}^\mathsf{T}\widetilde{\boldsymbol{\mathcal{D}}} + \mathbf{e}_\mathbf{v}^\mathsf{T}\mathbf{y}_\mathbf{f} + \mathbf{e}_\mathbf{p}^\mathsf{T}(\mathbf{h}+\mathbf{y}_\mathbf{p}) \\ & - \mathbf{y}_\mathbf{p}^\mathsf{T}\left(\boldsymbol{\zeta}_\mathbf{p}^{-1}\mathbf{y}_\mathbf{p} + \dot{\boldsymbol{\alpha}}\right) + \mathbf{y}_\mathbf{f}^\mathsf{T}\dot{\mathbf{y}}_\mathbf{f} - \widetilde{\boldsymbol{\mathcal{D}}}^\mathsf{T}\dot{\boldsymbol{\mathcal{D}}} \\ & - \frac{1}{m_o}\widetilde{\boldsymbol{\mathcal{D}}}^\mathsf{T}\mathbf{K}_{\boldsymbol{\eta}}(\widetilde{\boldsymbol{\Theta}}^\mathsf{T}\boldsymbol{\varpi}(\mathbf{Z}) + \widetilde{\boldsymbol{\mathcal{D}}}).\end{aligned} \tag{47}$$

Due to the fact that $\mathbf{y}_\mathbf{f} = \mathbf{f}_d - \bar{\mathbf{f}}_d$ and with the help of the filter (31), it follows that $\dot{\mathbf{y}}_\mathbf{f} = \dot{\mathbf{f}}_d - \dot{\bar{\mathbf{f}}}_d \implies \dot{\mathbf{y}}_\mathbf{f} = -\boldsymbol{\zeta}_\mathbf{v}^{-1}\mathbf{y}_\mathbf{f} - \dot{\bar{\mathbf{f}}}_d$. Therefore, (47) is written as

$$\begin{aligned}\dot{V}_2 =& -\mathbf{e}_\mathbf{p}^\mathsf{T}\mathbf{K}_1\mathbf{e}_\mathbf{p} - \mathbf{e}_\mathbf{v}^\mathsf{T}\mathbf{K}_2\mathbf{e}_\mathbf{v} - \mathbf{e}_\mathbf{v}^\mathsf{T}T_d\mathbf{S}^2(\mathbf{r}_3)\,\mathbf{r}_{3d} \\ & - \sigma\sum_{i=1}^{3}\widetilde{\boldsymbol{\Theta}}_i^\mathsf{T}\hat{\boldsymbol{\Theta}}_i - \mathbf{y}_\mathbf{p}^\mathsf{T}\left(\boldsymbol{\zeta}_\mathbf{p}^{-1}\mathbf{y}_\mathbf{p} + \dot{\boldsymbol{\alpha}}\right) - \mathbf{y}_\mathbf{f}^\mathsf{T}\left(\boldsymbol{\zeta}_\mathbf{v}^{-1}\mathbf{y}_\mathbf{f} + \dot{\bar{\mathbf{f}}}_d\right) \\ & - \mathbf{e}_\mathbf{v}^\mathsf{T}\widetilde{\boldsymbol{\mathcal{D}}} + \mathbf{e}_\mathbf{v}^\mathsf{T}\mathbf{y}_\mathbf{f} + \mathbf{e}_\mathbf{p}^\mathsf{T}(\mathbf{h}+\mathbf{y}_\mathbf{p}) - \widetilde{\boldsymbol{\mathcal{D}}}^\mathsf{T}\dot{\boldsymbol{\mathcal{D}}} \\ & - \frac{1}{m_o}\widetilde{\boldsymbol{\mathcal{D}}}^\mathsf{T}\mathbf{K}_{\boldsymbol{\eta}}(\widetilde{\boldsymbol{\Theta}}^\mathsf{T}\boldsymbol{\varpi}(\mathbf{Z}) + \widetilde{\boldsymbol{\mathcal{D}}}).\end{aligned} \tag{48}$$

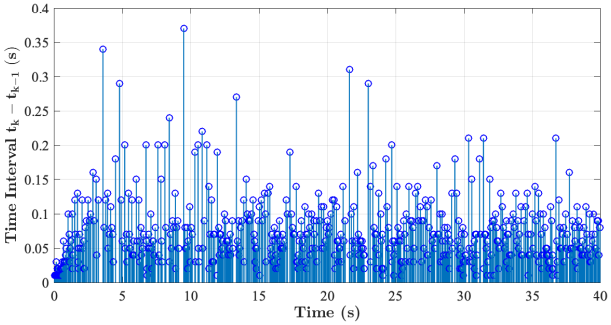

Figure 15. Consecutive time intervals for Case 2.

Part III: Then, our final Lyapunov function is introduced as

$$V_3 = V_2 + \frac{k_\mathbf{r}}{2}\mathbf{e}_\mathbf{r}^\mathsf{T}\mathbf{e}_\mathbf{r} = V_2 + k_\mathbf{r}\left(1 - \mathbf{r}_{3d}^\mathsf{T}\mathbf{r}_3\right), \tag{49}$$

where $\|\mathbf{r}_{3d}\| = \|\mathbf{r}_3\| = 1$ is employed. Using (1c) and (47), the derivative of V_3 w.r.t. time yields

$$\begin{aligned}\dot{V}_3 =& -\mathbf{e}_\mathbf{p}^\mathsf{T}\mathbf{K}_1\mathbf{e}_\mathbf{p} - \mathbf{e}_\mathbf{v}^\mathsf{T}\mathbf{K}_2\mathbf{e}_\mathbf{v} - \sigma\sum_{i=1}^{3}\widetilde{\boldsymbol{\Theta}}_i^\mathsf{T}\hat{\boldsymbol{\Theta}}_i + \mathbf{e}_\mathbf{p}^\mathsf{T}(\mathbf{h}+\mathbf{y}_\mathbf{p}) \\ & + k_\mathbf{r}\mathbf{r}_{3d}^\mathsf{T}\mathbf{R}\mathbf{S}(\mathbf{r}_3)\left(\boldsymbol{\Omega} - \mathbf{R}^\mathsf{T}\mathbf{S}(\mathbf{r}_{3d})\,\dot{\mathbf{r}}_{3d} - \frac{T_d}{k_\mathbf{r}}\mathbf{S}(\mathbf{e}_3)\,\mathbf{R}^\mathsf{T}\mathbf{e}_\mathbf{v}\right) \\ & - \mathbf{y}_\mathbf{p}^\mathsf{T}\left(\boldsymbol{\zeta}_\mathbf{p}^{-1}\mathbf{y}_\mathbf{p} + \dot{\boldsymbol{\alpha}}\right) - \mathbf{y}_\mathbf{f}^\mathsf{T}\left(\boldsymbol{\zeta}_\mathbf{v}^{-1}\mathbf{y}_\mathbf{f} + \dot{\bar{\mathbf{f}}}_d\right) - \mathbf{e}_\mathbf{v}^\mathsf{T}\widetilde{\mathcal{D}} + \mathbf{e}_\mathbf{v}^\mathsf{T}\mathbf{y}_\mathbf{f} \\ & - \widetilde{\boldsymbol{\mathcal{D}}}^\mathsf{T}\dot{\boldsymbol{\mathcal{D}}} - \frac{1}{m_o}\widetilde{\boldsymbol{\mathcal{D}}}^\mathsf{T}\mathbf{K}_{\boldsymbol{\eta}}\left(\widetilde{\boldsymbol{\Theta}}^\mathsf{T}\boldsymbol{\varpi}(\mathbf{Z}) + \widetilde{\boldsymbol{\mathcal{D}}}\right).\end{aligned} \tag{50}$$

Due to introducing the measure error $\mathbf{b}$, substituting (37) into (50) yields

$$\begin{aligned}\dot{V}_3 =& -\mathbf{e}_\mathbf{p}^\mathsf{T}\mathbf{K}_1\mathbf{e}_\mathbf{p} - \mathbf{e}_\mathbf{v}^\mathsf{T}\mathbf{K}_2\mathbf{e}_\mathbf{v} - \sigma\sum_{i=1}^{3}\widetilde{\boldsymbol{\Theta}}_i^\mathsf{T}\hat{\boldsymbol{\Theta}}_i - w_\mathbf{r}\|\mathbf{S}(\mathbf{r}_3)\,\mathbf{r}_{3d}\|^2 \\ & - \mathbf{y}_\mathbf{p}^\mathsf{T}\left(\boldsymbol{\zeta}_\mathbf{p}^{-1}\mathbf{y}_\mathbf{p} + \dot{\boldsymbol{\alpha}}\right) - \mathbf{y}_\mathbf{f}^\mathsf{T}\left(\boldsymbol{\zeta}_\mathbf{v}^{-1}\mathbf{y}_\mathbf{f} + \dot{\bar{\mathbf{f}}}_d\right) \\ & + k_\mathbf{r}\mathbf{r}_{3d}^\mathsf{T}\mathbf{R}\mathbf{S}(\mathbf{r}_3)\,\mathbf{b} - \mathbf{e}_\mathbf{v}^\mathsf{T}\widetilde{\boldsymbol{\mathcal{D}}} + \mathbf{e}_\mathbf{p}^\mathsf{T}(\mathbf{h}+\mathbf{y}_\mathbf{p}) - \widetilde{\boldsymbol{\mathcal{D}}}^\mathsf{T}\dot{\boldsymbol{\mathcal{D}}} \\ & - \frac{1}{m_o}\widetilde{\boldsymbol{\mathcal{D}}}^\mathsf{T}\mathbf{K}_{\boldsymbol{\eta}}\left(\widetilde{\boldsymbol{\Theta}}^\mathsf{T}\boldsymbol{\varpi}(\mathbf{Z}) + \widetilde{\boldsymbol{\mathcal{D}}}\right) + \mathbf{e}_\mathbf{v}^\mathsf{T}\mathbf{y}_\mathbf{f}.\end{aligned} \tag{51}$$

According to **Theorem 1**, we obtain that all the initial conditions of the quadrotor are bounded and satisfy $2V_3 \leq p_l$, where p_l is a positive constant, such that the set $\boldsymbol{\Pi}_v := \{V_3 : \mathbb{R}^{18+3l} \to \mathbb{R} |\ 2V_3 \leq p_l\}$ is compact in $\mathbb{R}^{18+3l}$. Since, for any positive constant B_o, the set $\boldsymbol{\Pi}_d := \{\left(\mathbf{p}_d^\mathsf{T}, \dot{\mathbf{p}}_d^\mathsf{T}, \ddot{\mathbf{p}}_d^\mathsf{T}\right) \in \mathbb{R}^9 |\ \|\mathbf{p}_d\| + \|\dot{\mathbf{p}}_d\| + \|\ddot{\mathbf{p}}_d\| \leq B_o\}$ is compact in $\mathbb{R}^9$. Therefore, $\boldsymbol{\Pi}_v \times \boldsymbol{\Pi}_d$ is compact in $\mathbb{R}^{27+3l}$, which implies that $\dot{\bar{\boldsymbol{\alpha}}}$ and $\dot{\bar{\mathbf{f}}}_d$ are norm-bounded, i.e., there exist positive constants α_c and f_c such that $\|\dot{\bar{\boldsymbol{\alpha}}}\| \leq \alpha_c$ and $\|\dot{\bar{\mathbf{f}}}_d\| \leq f_c$. According to **Assumption 1**, we have that the disturbance $\mathbf{d}$ is continuous and bounded, and therefore it is concluded that the compound disturbance $\boldsymbol{\mathcal{D}}$ is also continuous and bounded. With the help of **Lemma 2**, it is concluded that $\dot{\boldsymbol{\mathcal{D}}}$ is norm-bounded, i.e., there exists a positive constant (unknown) D_c such that $\|\dot{\boldsymbol{\mathcal{D}}}\| \leq D_c$. As a result, with the aid of the Young's inequality, it follows that $-\widetilde{\boldsymbol{\Theta}}_i^\mathsf{T}\hat{\boldsymbol{\Theta}}_i \leq -\frac{\delta_1^2}{2}\widetilde{\boldsymbol{\Theta}}_i^\mathsf{T}\widetilde{\boldsymbol{\Theta}}_i + \frac{1}{2\delta_1^2}\boldsymbol{\Theta}_i^\mathsf{T}\boldsymbol{\Theta}_i$, $i = 1,2,3$, $-\mathbf{y}_\mathbf{p}^\mathsf{T}\dot{\bar{\boldsymbol{\alpha}}} \leq \frac{1}{2}\mathbf{y}_\mathbf{p}^\mathsf{T}\mathbf{y}_\mathbf{p} + \frac{1}{2}\alpha_c^2$, $-\mathbf{y}_\mathbf{f}^\mathsf{T}\dot{\bar{\mathbf{f}}}_d \leq \frac{1}{2}\mathbf{y}_\mathbf{f}^\mathsf{T}\mathbf{y}_\mathbf{f} + \frac{1}{2}f_c^2$, $-\mathbf{e}_\mathbf{v}^\mathsf{T}\widetilde{\boldsymbol{\mathcal{D}}} \leq \frac{\delta_2^2}{2}\mathbf{e}_\mathbf{v}^\mathsf{T}\mathbf{e}_\mathbf{v} +$

$\frac{1}{2\delta_2^2}\widetilde{\boldsymbol{\mathcal{D}}}^{\mathsf{T}}\widetilde{\boldsymbol{\mathcal{D}}}$, $-\mathbf{e}_{\mathbf{v}}^{\mathsf{T}}(\mathbf{h}+\mathbf{y}_{\mathbf{p}}) \leq \delta_2^2\mathbf{e}_{\mathbf{v}}^{\mathsf{T}}\mathbf{e}_{\mathbf{v}} + \frac{1}{2\delta_2^2}\left(\bar{h}^2+\mathbf{y}_{\mathbf{p}}^{\mathsf{T}}\mathbf{y}_{\mathbf{p}}\right)$, $-\widetilde{\boldsymbol{\mathcal{D}}}^{\mathsf{T}}\dot{\boldsymbol{\mathcal{D}}} \leq \frac{1}{2}\widetilde{\boldsymbol{\mathcal{D}}}^{\mathsf{T}}\widetilde{\boldsymbol{\mathcal{D}}} + \frac{1}{2}D_c^2$, $-\frac{1}{m_o}\widetilde{\boldsymbol{\mathcal{D}}}^{\mathsf{T}}\mathbf{K}_{\boldsymbol{\eta}}\left(\widetilde{\boldsymbol{\Theta}}^{\mathsf{T}}\boldsymbol{\varpi}(\mathbf{Z})+\widetilde{\boldsymbol{\mathcal{D}}}\right) \leq \frac{1}{m_o}\widetilde{\boldsymbol{\mathcal{D}}}^{\mathsf{T}}\left(\frac{\delta_3^2}{2}\mathbf{K}_{\boldsymbol{\eta}}\mathbf{K}_{\boldsymbol{\eta}}^{\mathsf{T}}-\mathbf{K}_{\boldsymbol{\eta}}\right)\widetilde{\boldsymbol{\mathcal{D}}} + \frac{1}{2\delta_3^2 m_o}\|\boldsymbol{\varpi}(\mathbf{Z})\|^2\sum_{i=1}^{3}\widetilde{\boldsymbol{\Theta}}_i^{\mathsf{T}}\widetilde{\boldsymbol{\Theta}}_i$, and $\mathbf{e}_{\mathbf{v}}^{\mathsf{T}}\mathbf{y}_{\mathbf{f}} \leq \frac{\delta_2^2}{2}\mathbf{e}_{\mathbf{v}}^{\mathsf{T}}\mathbf{e}_{\mathbf{v}} + \frac{1}{2\delta_2^2}\mathbf{y}_{\mathbf{f}}^{\mathsf{T}}\mathbf{y}_{\mathbf{f}}$, where δ_1, δ_2, $\delta_3 > 0$. Since $\|\mathbf{r}_{3d}\| = 1$, $\|\mathbf{R}\| = \sqrt{3}$, and $\|\mathbf{S}(\mathbf{r}_3)\| = \sqrt{2}$ using the Frobenius norm, it will follow that $k_{\mathbf{r}}\mathbf{r}_{3d}^{\mathsf{T}}\mathbf{R}\mathbf{S}(\mathbf{r}_3)\,\mathbf{b} \leq -\frac{k_{\mathbf{r}}}{2\delta_4^2}\mathbf{r}_{3d}^{\mathsf{T}}\mathbf{R}\mathbf{S}^2(\mathbf{r}_3)\,\mathbf{R}^{\mathsf{T}}\mathbf{r}_{3d} + \frac{k_{\mathbf{r}}\delta_4^2}{2}\mathbf{b}^{\mathsf{T}}\mathbf{b} \implies k_{\mathbf{r}}\mathbf{r}_{3d}^{\mathsf{T}}\mathbf{R}\mathbf{S}(\mathbf{r}_3)\,\mathbf{b} \leq \frac{3k_{\mathbf{r}}}{\delta_4^2} + \frac{k_{\mathbf{r}}\delta_4^2}{2}\mathbf{b}^{\mathsf{T}}\mathbf{b}$, where $\delta_4 > 0$.

Based on the above inequalities, a bound of $\dot{V}_3$ in (51) is

$$\begin{aligned}\dot{V}_3 \leq & -\mathbf{e}_{\mathbf{p}}^{\mathsf{T}}\mathbf{K}_1\mathbf{e}_{\mathbf{p}} - \mathbf{e}_{\mathbf{v}}^{\mathsf{T}}\left(\mathbf{K}_2 - 2\delta_2^2\mathbf{I}\right)\mathbf{e}_{\mathbf{v}} - w_{\mathbf{r}}\|\mathbf{S}(\mathbf{r}_3)\,\mathbf{r}_{3d}\|^2 \\ & - \frac{1}{2}\left(\sigma\delta_1^2 - \frac{\|\boldsymbol{\varpi}(\mathbf{Z})\|^2}{\delta_3^2 m_o}\right)\sum_{i=1}^{3}\widetilde{\boldsymbol{\Theta}}_i^{\mathsf{T}}\widetilde{\boldsymbol{\Theta}}_i \\ & - \mathbf{y}_{\mathbf{p}}^{\mathsf{T}}\left(\boldsymbol{\zeta}_{\mathbf{p}}^{-1} - \frac{1}{2}(1+\frac{1}{\delta_2^2})\mathbf{I}\right)\mathbf{y}_{\mathbf{p}} + \frac{3k_{\mathbf{r}}}{\delta_4^2} + \frac{k_{\mathbf{r}}\delta_4^2}{2}\mathbf{b}^{\mathsf{T}}\mathbf{b} \\ & - \mathbf{y}_{\mathbf{f}}^{\mathsf{T}}\left(\boldsymbol{\zeta}_{\mathbf{v}}^{-1} - \frac{1}{2}(1+\frac{1}{\delta_2^2})\mathbf{I}\right)\mathbf{y}_{\mathbf{f}} + \frac{\sigma}{2\delta_1^2}\sum_{i=1}^{3}\boldsymbol{\Theta}_i^{\mathsf{T}}\boldsymbol{\Theta}_i \\ & - \widetilde{\boldsymbol{\mathcal{D}}}^{\mathsf{T}}\left(\frac{1}{m_o}\mathbf{K}_{\boldsymbol{\eta}} - \frac{\delta_3^2}{2m_o}\mathbf{K}_{\boldsymbol{\eta}}\mathbf{K}_{\boldsymbol{\eta}}^{\mathsf{T}} - \frac{1}{2}(1+\frac{1}{\delta_2^2})\mathbf{I}\right)\widetilde{\boldsymbol{\mathcal{D}}} \\ & + \frac{1}{2}\left(\alpha_c^2 + f_c^2 + \frac{1}{\delta_2^2}\bar{h}^2 + D_c^2\right). \end{aligned} \tag{52}$$

Remark 9. *For a quadrotor UAV, the measurement error* $\mathbf{b}$ *must not be too large. If the measurement error* $\mathbf{b}$ *is too large, it implies that the actuator cannot generate a sufficiently high angular velocity to maintain system stability [48]. Considering the controllability of a practical system, it is reasonable to assume that* $\mathbf{b}$ *is bounded by a constant, specifically* $\|\mathbf{b}\| \leq \bar{b}$ *with* $\bar{b} > 0$.

With the help of **Remark 9**, (52) is written as

$$\begin{aligned}\dot{V}_3 \leq & -\mathbf{e}_{\mathbf{p}}^{\mathsf{T}}\mathbf{A}_1\mathbf{e}_{\mathbf{p}} - \mathbf{e}_{\mathbf{v}}^{\mathsf{T}}\mathbf{A}_2\mathbf{e}_{\mathbf{v}} - a_3\|\mathbf{S}(\mathbf{r}_3)\,\mathbf{r}_{3d}\|^2 - a_4\sum_{i=1}^{3}\widetilde{\boldsymbol{\Theta}}_i^{\mathsf{T}}\widetilde{\boldsymbol{\Theta}}_i \\ & - \mathbf{y}_{\mathbf{p}}^{\mathsf{T}}\mathbf{A}_5\mathbf{y}_{\mathbf{p}} - \mathbf{y}_{\mathbf{f}}^{\mathsf{T}}\mathbf{A}_6\mathbf{y}_{\mathbf{f}} - \widetilde{\boldsymbol{\mathcal{D}}}^{\mathsf{T}}\mathbf{A}_7\widetilde{\boldsymbol{\mathcal{D}}} + C, \end{aligned} \tag{53}$$

where $\mathbf{A}_1 := \mathbf{K}_1 \in \mathbb{R}^{3\times3}$, $\mathbf{A}_2 := \mathbf{K}_2 - 2\delta_2^2\mathbf{I} \in \mathbb{R}^{3\times3}$, $a_3 := w_{\mathbf{r}} \in \mathbb{R}$, $a_4 := \frac{1}{2}\left(\sigma\delta_1^2 - \frac{\|\boldsymbol{\varpi}(\mathbf{Z})\|^2}{\delta_3^2 m_o}\right) \in \mathbb{R}$, $\mathbf{A}_5 := \boldsymbol{\zeta}_{\mathbf{p}}^{-1} - \frac{1}{2}(1+\frac{1}{\delta_2^2})\mathbf{I} \in \mathbb{R}^{3\times3}$, $\mathbf{A}_6 := \boldsymbol{\zeta}_{\mathbf{v}}^{-1} - \frac{1}{2}(1+\frac{1}{\delta_2^2})\mathbf{I} \in \mathbb{R}^{3\times3}$, $\mathbf{A}_7 := \frac{1}{m_o}\mathbf{K}_{\boldsymbol{\eta}} - \frac{\delta_3^2}{2m_o}\mathbf{K}_{\boldsymbol{\eta}}\mathbf{K}_{\boldsymbol{\eta}}^{\mathsf{T}} - \frac{1}{2}(1+\frac{1}{\delta_2^2})\mathbf{I} \in \mathbb{R}^{3\times3}$, and $C = \frac{\sigma}{2\delta_1^2}\sum_{i=1}^{3}\boldsymbol{\Theta}_i^{\mathsf{T}}\boldsymbol{\Theta}_i + \frac{1}{2}\left(\alpha_c^2 + f_c^2 + \frac{1}{\delta_2^2}\bar{h}^2 + D_c^2\right) + \frac{3k_{\mathbf{r}}}{\delta_4^2} + \frac{k_{\mathbf{r}}\delta_4^2}{2}\bar{b}^2 \in \mathbb{R}$.

Controller gains $\mathbf{K}_1$, $\mathbf{K}_2$, σ, $\boldsymbol{\zeta}_{\mathbf{v}}$, $\boldsymbol{\zeta}_{\mathbf{p}}$, $k_{\mathbf{r}}$, $\omega_{\mathbf{r}}$ and disturbance observer gains $\mathbf{K}_{\boldsymbol{\eta}}$ as well as the parameters δ_i, $i = 1,\ldots,4$, should be properly selected in practice to satisfy $\mathbf{A}_1$, $\mathbf{A}_2$, $\mathbf{A}_5$, $\mathbf{A}_6$, $\mathbf{A}_7 \succ 0$ and a_3, a_4, $C > 0$. It should be emphasized that the parameters δ_i, $i = 1,\ldots,4$, are not control design parameter and are solely auxiliary analysis variables related with the positive definition of the above variables.

Define the total error of the closed-loop system as

$$\begin{aligned}\boldsymbol{\Psi} := \Big[& \mathbf{e}_{\mathbf{p}}^{\mathsf{T}}, \sqrt{m_o}\mathbf{e}_{\mathbf{v}}^{\mathsf{T}}, \boldsymbol{\Gamma}^{-\frac{1}{2}}\widetilde{\boldsymbol{\Theta}}_1^{\mathsf{T}}, \boldsymbol{\Gamma}^{-\frac{1}{2}}\widetilde{\boldsymbol{\Theta}}_2^{\mathsf{T}}, \boldsymbol{\Gamma}^{-\frac{1}{2}}\widetilde{\boldsymbol{\Theta}}_3^{\mathsf{T}}, \widetilde{\boldsymbol{\mathcal{D}}}^{\mathsf{T}}, \mathbf{y}_{\mathbf{p}}^{\mathsf{T}}, \\ & \mathbf{y}_{\mathbf{f}}^{\mathsf{T}}, \sqrt{\frac{k_{\mathbf{r}}}{2}}\mathbf{e}_{\mathbf{r}}^{\mathsf{T}}\mathbf{S}^2(\mathbf{r}_3) \Big]^{\mathsf{T}} \in \mathbb{R}^{18+3l}, \end{aligned} \tag{54}$$

and $\|\boldsymbol{\Psi}\|^2 = \mathbf{e}_{\mathbf{p}}^{\mathsf{T}}\mathbf{e}_{\mathbf{p}} + m_o\mathbf{e}_{\mathbf{v}}^{\mathsf{T}}\mathbf{e}_{\mathbf{v}} + \sum_{i=1}^{3}\widetilde{\boldsymbol{\Theta}}_i^{\mathsf{T}}\boldsymbol{\Gamma}^{-1}\widetilde{\boldsymbol{\Theta}}_i + \widetilde{\boldsymbol{\mathcal{D}}}^{\mathsf{T}}\widetilde{\boldsymbol{\mathcal{D}}} + \mathbf{y}_{\mathbf{p}}^{\mathsf{T}}\mathbf{y}_{\mathbf{p}} + \mathbf{y}_{\mathbf{f}}^{\mathsf{T}}\mathbf{y}_{\mathbf{f}} - \frac{k_{\mathbf{r}}}{2}\mathbf{e}_{\mathbf{r}}^{\mathsf{T}}\mathbf{S}^2(\mathbf{r}_3)\,\mathbf{e}_{\mathbf{r}}$. Since $\|\mathbf{S}(\mathbf{r}_3)\| = \sqrt{2}$ using the Frobenius norm, it follows that $\|\boldsymbol{\Psi}\|^2 \leq \mathbf{e}_{\mathbf{p}}^{\mathsf{T}}\mathbf{e}_{\mathbf{p}} + m_o\mathbf{e}_{\mathbf{v}}^{\mathsf{T}}\mathbf{e}_{\mathbf{v}} + \sum_{i=1}^{3}\widetilde{\boldsymbol{\Theta}}_i^{\mathsf{T}}\boldsymbol{\Gamma}^{-1}\widetilde{\boldsymbol{\Theta}}_i + \widetilde{\boldsymbol{\mathcal{D}}}^{\mathsf{T}}\widetilde{\boldsymbol{\mathcal{D}}} + \mathbf{y}_{\mathbf{p}}^{\mathsf{T}}\mathbf{y}_{\mathbf{p}} + \mathbf{y}_{\mathbf{f}}^{\mathsf{T}}\mathbf{y}_{\mathbf{f}} + k_{\mathbf{r}}\mathbf{e}_{\mathbf{r}}^{\mathsf{T}}\mathbf{e}_{\mathbf{r}} = 2V_3$, which implies that $\|\boldsymbol{\Psi}\|^2 \leq 2V_3 \leq p_l$. Furthermore, let us define an auxiliary block-diagonal matrix given by $\boldsymbol{\Pi} := \text{blkdiag}(\mathbf{A}_1, \frac{1}{m_o}\mathbf{A}_2, a_4\boldsymbol{\Gamma}, a_4\boldsymbol{\Gamma}, a_4\boldsymbol{\Gamma}, \mathbf{A}_7, \mathbf{A}_5, \mathbf{A}_6, \frac{2a_3}{k_{\mathbf{r}}}\mathbf{I}) \in \mathbb{R}^{(18+3l)\times(18+3l)}$. Obviously, $\boldsymbol{\Pi} \succ 0$. As a result, using the above definition, (53) is written as

$$\dot{V}_3 \leq -\boldsymbol{\Psi}^{\mathsf{T}}\boldsymbol{\Pi}\boldsymbol{\Psi} + C \leq -\lambda_{\min}(\boldsymbol{\Pi})\|\boldsymbol{\Psi}\|^2 + C, \tag{55}$$

where $\lambda_{\min}(\boldsymbol{\Pi})$ is the minimum eigenvalue of the matrix $\boldsymbol{\Pi}$. In addition, from (55), it is found that as $\lambda_{\min}(\boldsymbol{\Pi}) > \frac{C}{p_l}$, $\dot{V}_3 < 0$ on $\|\boldsymbol{\Psi}\|^2 = p_l$. Thus, the set $\boldsymbol{\Pi}_v$ is an invariant set, i.e., if $2V_3(0) \leq p_l$, then $2V_3(t) \leq p_l$ for all $t > 0$, which implies that the total error of the closed-loop system, $\boldsymbol{\Psi}$, is UUB. According to the definition of $\boldsymbol{\Psi}$, it is concluded that the errors $\mathbf{e}_{\mathbf{p}}$, $\mathbf{e}_{\mathbf{v}}$, $\widetilde{\boldsymbol{\Theta}}_i$, $i = 1,2,3$, $\widetilde{\boldsymbol{\mathcal{D}}}$, $\mathbf{y}_{\mathbf{p}}$, $\mathbf{y}_{\mathbf{f}}$ and $\mathbf{e}_{\mathbf{r}}$ are UUB, which completes the proof.

REFERENCES

[1] Z. Zhao, J. Zhang, Z. Liu, W. He, and K.-S. Hong, "Adaptive quantized fault-tolerant control of a 2-dof helicopter system with actuator fault and unknown dead zone," *Automatica*, vol. 148, p. 110792, 2023.

[2] Y. Wang, Y. Wang, and B. Ren, "Energy saving quadrotor control for field inspections," *IEEE Transactions on Systems, Man, and Cybernetics: Systems*, vol. 52, no. 3, pp. 1768–1777, 2022.

[3] L.-X. Xu, H.-J. Ma, D. Guo, A.-H. Xie, and D.-L. Song, "Backstepping sliding-mode and cascade active disturbance rejection control for a quadrotor uav," *IEEE/ASME Transactions on Mechatronics*, vol. 25, no. 6, pp. 2743–2753, 2020.

[4] X. Liang, Z. Zhang, H. Yu, Y. Wang, Y. Fang, and J. Han, "Antiswing control for aerial transportation of the suspended cargo by dual quadrotor uavs," *IEEE/ASME Transactions on Mechatronics*, vol. 27, no. 6, pp. 5159–5172, 2022.

[5] K. Zhao, J. Zhang, D. Ma, and Y. Xia, "Composite disturbance rejection attitude control for quadrotor with unknown disturbance," *IEEE Transactions on Industrial Electronics*, vol. 67, no. 8, pp. 6894–6903, 2020.

[6] A. Roberts and A. Tayebi, "Adaptive position tracking of vtol uavs," *IEEE Transactions on Robotics*, vol. 27, no. 1, pp. 129–142, 2011.

[7] A. Roberts and A. Tayebi, "A new position regulation strategy for vtol uavs using imu and gps measurements," *Automatica*, vol. 49, no. 2, pp. 434–440, 2013.

[8] A. Abdessameud and A. Tayebi, "Global trajectory tracking control of vtol-uavs without linear velocity measurements," *Automatica*, vol. 46, no. 6, pp. 1053–1059, 2010.

[9] D. Invernizzi and M. Lovera, "Trajectory tracking control of thrust-vectoring uavs," *Automatica*, vol. 95, pp. 180–186, 2018.

[10] M. Mehndiratta, E. Kayacan, M. Reyhanoglu, and E. Kayacan, "Robust tracking control of aerial robots via a simple learning strategy-based feedback linearization," *IEEE Access*, vol. 8, pp. 1653–1669, 2020.

[11] M. Mehndiratta and E. Kayacan, "A constrained instantaneous learning approach for aerial package delivery robots: onboard implementation and experimental results," *Autonomous Robots*, vol. 43, pp. 2209–2228, 2019.

[12] P. Bouffard, A. Aswani, and C. Tomlin, "Learning-based model predictive control on a quadrotor: Onboard implementation and experimental results," in *2012 IEEE International Conference on Robotics and Automation*, pp. 279–284, 2012.

[13] Y. Wang, L. Zheng, H. Zhang, and W. X. Zheng, "Fuzzy observer-based repetitive tracking control for nonlinear systems," *IEEE Transactions on Fuzzy Systems*, vol. 28, no. 10, pp. 2401–2415, 2020.

[14] Y. Li, X. Min, and S. Tong, "Observer-based fuzzy adaptive inverse optimal output feedback control for uncertain nonlinear systems," *IEEE Transactions on Fuzzy Systems*, vol. 29, no. 6, pp. 1484–1495, 2021.

[15] S. Lu, M. Chen, Y. Liu, and S. Shao, "Adaptive nn tracking control for uncertain mimo nonlinear system with time-varying state constraints and disturbances," *IEEE Transactions on Neural Networks and Learning Systems*, vol. 34, no. 10, pp. 7309–7323, 2023.

[16] G. Wang, Y. Chen, P. An, H. Hong, J. Hu, and T. Huang, "Uav-yolov8: A small-object-detection model based on improved yolov8 for uav aerial photography scenarios," *Sensors*, vol. 23, no. 16, 2023.

[17] J. Gu, T. Su, Q. Wang, X. Du, and M. Guizani, "Multiple moving targets surveillance based on a cooperative network for multi-uav," *IEEE Communications Magazine*, vol. 56, no. 4, pp. 82–89, 2018.

[18] B. Zhao, B. Xian, Y. Zhang, and X. Zhang, "Nonlinear robust adaptive tracking control of a quadrotor uav via immersion and invariance methodology," *IEEE Transactions on Industrial Electronics*, vol. 62, no. 5, pp. 2891–2902, 2015.

[19] L. Kong, J. Reis, W. He, and C. Silvestre, "Comprehensive nonlinear control strategy for vtol-uavs with windowed output constraints," *IEEE Transactions on Control Systems Technology*, vol. 31, no. 6, pp. 2673–2684, 2023.

[20] L. Kong, J. Reis, W. He, and C. Silvestre, "Experimental validation of a robust prescribed performance nonlinear controller for an unmanned aerial vehicle with unknown mass," *IEEE/ASME Transactions on Mechatronics*, vol. 29, no. 1, pp. 301–312, 2024.

[21] W. Xie, D. Cabecinhas, R. Cunha, and C. Silvestre, "Adaptive backstepping control of a quadcopter with uncertain vehicle mass, moment of inertia, and disturbances," *IEEE Transactions on Industrial Electronics*, vol. 69, no. 1, pp. 549–559, 2022.

[22] G. Chen, D. Yao, H. Li, Q. Zhou, and R. Lu, "Saturated threshold event-triggered control for multiagent systems under sensor attacks and its application to uavs," *IEEE Transactions on Circuits and Systems I: Regular Papers*, vol. 69, no. 2, pp. 884–895, 2022.

[23] L. Xing, C. Wen, Z. Liu, H. Su, and J. Cai, "Event-triggered adaptive control for a class of uncertain nonlinear systems," *IEEE Transactions on Automatic Control*, vol. 62, no. 4, pp. 2071–2076, 2017.

[24] J. Qiu, K. Sun, T. Wang, and H. Gao, "Observer-based fuzzy adaptive event-triggered control for pure-feedback nonlinear systems with prescribed performance," *IEEE Transactions on Fuzzy Systems*, vol. 27, no. 11, pp. 2152–2162, 2019.

[25] C.-H. Zhang and G.-H. Yang, "Event-triggered global finite-time control for a class of uncertain nonlinear systems," *IEEE Transactions on Automatic Control*, vol. 65, no. 3, pp. 1340–1347, 2020.

[26] H. Ma, Q. Zhou, H. Li, and R. Lu, "Adaptive prescribed performance control of a flexible-joint robotic manipulator with dynamic uncertainties," *IEEE Transactions on Cybernetics*, vol. 52, no. 12, pp. 12905–12915, 2022.

[27] X. Ge, Q.-L. Han, X.-M. Zhang, and D. Ding, "Dynamic event-triggered control and estimation: A survey," *International Journal of Automation and Computing*, vol. 18, no. 6, pp. 857–886, 2021.

[28] Y. Zhang, Z.-G. Wu, and P. Shi, "Resilient event-/self-triggering leader-following consensus control of multiagent systems against dos attacks," *IEEE Transactions on Industrial Informatics*, vol. 19, no. 4, pp. 5925–5934, 2023.

[29] Y. Pan, P. Du, H. Xue, and H.-K. Lam, "Singularity-free fixed-time fuzzy control for robotic systems with user-defined performance," *IEEE Transactions on Fuzzy Systems*, vol. 29, no. 8, pp. 2388–2398, 2021.

[30] Z. Liu, J. Shi, Y. He, Z. Zhao, and H.-K. Lam, "Adaptive fuzzy control for a spatial flexible hose system with dynamic event-triggered mechanism," *IEEE Transactions on Aerospace and Electronic Systems*, vol. 59, no. 2, pp. 1156–1167, 2023.

[31] Z. Xu, Z.-G. Wu, H. Que, and P. Jiang, "Asynchronous control of nonlinear markov jump systems with uncertainties using interval type-2 polynomial fuzzy approach," *IEEE Transactions on Fuzzy Systems*, 2023, in press, doi: 10.1109/TFUZZ.2023.3311811.

[32] Y. Li, Y. Zhao, W. Liu, and J. Hu, "Adaptive fuzzy predefined-time control for third-order heterogeneous vehicular platoon systems with dead zone," *IEEE Transactions on Industrial Informatics*, vol. 19, no. 9, pp. 9525–9534, 2023.

[33] X. Zhang, Y. Wang, G. Zhu, X. Chen, Z. Li, C. Wang, and C.-Y. Su, "Compound adaptive fuzzy quantized control for quadrotor and its experimental verification," *IEEE Transactions on Cybernetics*, vol. 51, no. 3, pp. 1121–1133, 2021.

[34] A. S. Huaman Loayza and C. G. Pérez Zuñiga, "Design of a fuzzy sliding mode controller for the autonomous path-following of a quadrotor," *IEEE Latin America Transactions*, vol. 17, no. 06, pp. 962–971, 2019.

[35] W. Liu, X. Cheng, and J. Zhang, "Command filter-based adaptive fuzzy integral backstepping control for quadrotor uav with input saturation," *Journal of the Franklin Institute*, vol. 360, no. 1, pp. 484–507, 2023.

[36] Q. Chen, M. Tao, X. He, and L. Tao, "Fuzzy adaptive nonsingular fixed-time attitude tracking control of quadrotor uavs," *IEEE Transactions on Aerospace and Electronic Systems*, vol. 57, no. 5, pp. 2864–2877, 2021.

[37] A. Roberts and A. Tayebi, "A new position regulation strategy for vtol uavs using imu and gps measurements," *Automatica*, vol. 49, no. 2, pp. 434–440, 2013.

[38] M. Mehndiratta, E. Kayacan, M. Reyhanoglu, and E. Kayacan, "Robust tracking control of aerial robots via a simple learning strategy-based feedback linearization," *Ieee Access*, vol. 8, pp. 1653–1669, 2019.

[39] S. BEHTASH, "Robust output tracking for non-linear systems," *International Journal of Control*, vol. 51, no. 6, pp. 1381–1407, 1990.

[40] Z. Li, C.-Y. Su, L. Wang, Z. Chen, and T. Chai, "Nonlinear disturbance observer-based control design for a robotic exoskeleton incorporating fuzzy approximation," *IEEE Transactions on Industrial Electronics*, vol. 62, no. 9, pp. 5763–5775, 2015.

[41] D. Cui and Z. Xiang, "Nonsingular fixed-time fault-tolerant fuzzy control for switched uncertain nonlinear systems," *IEEE Transactions on Fuzzy Systems*, vol. 31, no. 1, pp. 174–183, 2023.

[42] C. P. Bechlioulis and G. A. Rovithakis, "A low-complexity global approximation-free control scheme with prescribed performance for unknown pure feedback systems," *Automatica*, vol. 50, no. 4, pp. 1217–1226, 2014.

[43] I. D. Landau, R. Lozano, M. M'Saad, *et al.*, *Adaptive control*. Springer New York, 1998.

[44] L. Xing and C. Wen, "Dynamic event-triggered adaptive control for a class of uncertain nonlinear systems," *Automatica*, vol. 158, p. 111286, 2023.

[45] H. Ma, H. Li, R. Lu, and T. Huang, "Adaptive event-triggered control for a class of nonlinear systems with periodic disturbances," *Science China Information Sciences*, vol. 63, pp. 1–15, 2020.

[46] L. Cao, Z. Cheng, Y. Liu, and H. Li, "Event-based adaptive nn fixed-time cooperative formation for multiagent systems," *IEEE Transactions on Neural Networks and Learning Systems*, 2022, in press, doi: 10.1109/TNNLS.2022.3210269.

[47] D. Wang and J. Huang, "Neural network-based adaptive dynamic surface control for a class of uncertain nonlinear systems in strict-feedback form," *IEEE Transactions on Neural Networks*, vol. 16, no. 1, pp. 195–202, 2005.

[48] L. Sun and Z. Zheng, "Disturbance-observer-based robust backstepping attitude stabilization of spacecraft under input saturation and measurement uncertainty," *IEEE Transactions on Industrial Electronics*, vol. 64, no. 10, pp. 7994–8002, 2017.

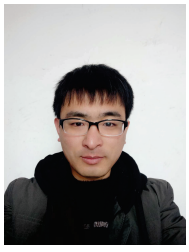

Linghuan Kong received the M.Eng. degree from the School of Automation Engineering, University of Electronic Science and Technology of China, Chengdu, China, in 2019, and the Ph.D. degree from the School of Intelligence Science and Technology, University of Science and Technology Beijing, Beijing, China, in 2023. He was a Research Assistant with the Faculty of Science and Technology, University of Macau, from September 2021 to October 2022. He is currently a Post-Doctoral Fellow with the Faculty of Science and Technology, University of Macau. His current research interests include robotics, unmanned aerial vehicles, adaptive and learning control.

Zhijie Liu received B.Sc. degree in automation from China University of Mining and Technology Beijing, Beijing, China in 2014, and the Ph.D degree in control science and engineering from Beihang University, Beijing, China in 2019. In 2017, he was a Research Assistant with the Department of Electrical Engineering, University of Notre Dame, for twelve months. He is currently a Full Professor with School of Intelligence Science and Technology, University of Science and Technology Beijing (USTB), Beijing, China. His research interests include adaptive control, modeling and vibration control for flexible structures, and distributed parameter system.

Zhijia Zhao (Member, IEEE) received the B.Eng. degree in automatic control from the North China University of Water Resources and Electric Power, Zhengzhou, China, in 2010, and the M.Eng. and Ph.D. degrees in automatic control from the South China University of Technology, Guangzhou, China, in 2013 and 2017, respectively. He is currently a Professor with the School of Mechanical and Electrical Engineering, Guangzhou University, Guangzhou. His research interests include adaptive and learning control, flexible mechanical systems, and robotics.

Hak-Keung Lam (Fellow, IEEE) received the B.Eng. (Hons.) and Ph.D. degrees from the Department of Electronic and Information Engineering, Hong Kong Polytechnic University, Hong Kong, in 1995 and 2000, respectively. From 2000 and 2005, he was with the Department of Electronic and Information Engineering, Hong Kong Polytechnic University as a Postdoctoral Fellow and a Research Fellow, respectively. In 2005, he joined as a Lecturer with Kings College London, London, U.K., where he is currently a Reader. He has coedited two edited volumes: Control of Chaotic Nonlinear Circuits (World Scientific, 2009) and Computational Intelligence and Its Applications (World Scientific, 2012), and authored/coauthored three monographs: Stability Analysis of Fuzzy-Model-Based Control Systems (Springer, 2011), Polynomial Fuzzy Model-Based Control Systems (Springer, 2016), and Analysis and Synthesis for Interval Type-2 Fuzzy-Model-Based Systems (Springer, 2016). His current research interests include intelligent control and computational intelligence., Dr. Lam is currently the Program Committee Member, the International Advisory Board Member, the Invited Session Chair, and the Publication Chair for various international conferences, and a Reviewer for various books, international journals, and international conferences. He was an Associate Editor for IEEE Transactions on Circuits and Systems Part II: Express Briefs and currently an Associate Editor for IEEE Transactions on Fuzzy Systems, IET Control Theory and Applications, International Journal of Fuzzy Systems, Neurocomputing, and Nonlinear Dynamics, and a Guest Editor/Editorial Board for a number of international journals. He was named as a highly cited Researcher by the Web of Science.